Diploma Thesis

Distributed Secondary Control in Microgrids

Hedi Bouattour

May 10, 2013

Betreuer:
Florian Dörfler

University of California, Santa Barbara
Center for Control, Dynamical Systems and Computation
Prof. Francesco Bullo

Institut für Systemtheorie und Regelungstechnik
Universität Stuttgart
Prof. Dr.-Ing. Frank Allgöwer

Contents

1 Introduction **1**
- 1.1 Microgrids and Control . . . 1
- 1.2 Literature review . . . 2
- 1.3 Contributions and Structure . . . 4

2 Definitions and Problem Setup **5**
- 2.1 Power Inverters and Droop Control . . . 5
- 2.2 Notation and Geometric Definitions . . . 6
- 2.3 Algebraic Graph Theory . . . 7
- 2.4 Active Power Flow in AC networks . . . 8
- 2.5 Droop-Controlled Microgrid . . . 9
- 2.6 General Simulation Setup . . . 12

3 Secondary Control Strategies in a Microgrid **15**
- 3.1 Distributed Averaging PI Control . . . 16
- 3.2 Centralized Averaging PI Control . . . 19
- 3.3 Optimal Distributed Averaging PI Control . . . 26

4 Extensions to Secondary Control **31**
- 4.1 Extension of DAPI/CAPI Control to Lossy Networks . . . 31
  - 4.1.1 Existence and Uniqueness of Synchronized Solutions . . . 31
  - 4.1.2 Stability of Unique Synchronized Solutions . . . 34
  - 4.1.3 Injection Constraints and Power Sharing in Lossy Networks . . . 35
- 4.2 Partial DAPI/CAPI Control . . . 36
  - 4.2.1 Stability of Partial Secondary-Controlled Network . . . 37
  - 4.2.2 Injection Constraints and Power Sharing . . . 37

5 Conclusions **41**
- 5.1 Summary . . . 41
- 5.2 Possible Future Work . . . 41

Eidesstattliche Erklärung

Ich versichere hiermit, dass ich, Hedi Bouattour, die vorliegende Arbeit selbstständig angefertigt, keine anderen als die angegebenen Hilfsmittel benutzt und sowohl wörtliche, als auch sinngemäß entlehnte Stellen als solche kenntlich gemacht habe. Die Arbeit hat in gleicher oder ähnlicher Form noch keiner anderen Prüfungsbehörde vorgelegen.

Ort, Datum	Unterschrift

Abstract

The recent changes in the structure of power generation towards a distributed generation have motivated the increasing interest in the control of so-called microgrids. Microgrids typically consist of an AC electrical network connecting a set of loads and droop-controlled inverters. While the decentralized and proportional primary droop-control ensures the stabilization and the synchronization of the inverters frequencies, the purpose of secondary control strategies is to regulate the frequencies to a rated value. In this work, we build on recent necessary and sufficient stability conditions for an inductive microgrid and propose several analysis and design results for two distributed secondary control schemes: a Distributed Averaging PI (DAPI) controller and a Centralized Averaging PI (CAPI) controller. We will show that both controllers achieve frequency regulation in the presence of power losses in network, even when the secondary control action is restricted to a subset of inverters. We will also prove that the controllers minimize a quadratic cost function of the secondary-power generation for a proper selection of the droop coefficients.

Kurzfassung

Die jüngsten Wandel in der Struktur der Stromerzeugung von einer zentralen Erzeugung hin zu einer dezentralen Erzeugung regen das wachsende Interesse an der Regelung der sogenannten Microgrids an. Microgrids sind in der Regel synchrone elektrische Wechselstromnetze, die Wechselrichter und Lasten miteinander verbinden. Während sich die dezentrale proportionale Primärregelung um die Synchronisierung der Wechselrichterfrequenzen kümmert, hat die Sekundärregelung die Aufgabe, bleibende Frequenzabweichungen auszuregeln. Ausgehend von neuen notwendingen und hinreichenden parametrischen Stabilitätsbedingungen für ein induktives droopgeregeltes Microgrid untersucht diese Arbeit die Stabilität zweier verteilter Sekundärregler, eines verteilten mittelwertbildenden PI (DAPI) Reglers und eines zentralen mittelwertbildenden PI (CAPI) Reglers. Es wird gezeigt, dass beide Regler Frequenzabweichungen in verlustbehafteten Netzwerken erfolgreich ausregeln, auch wenn sich nur eine Untermenge der Wechselrichter an der Sekundärregelung beteiligt. Es wird auch gezeigt, dass diese Regeler dabei eine proportionale Aufteilung der abzudeckenden Last unter den sich an der Sekundärregelung beteiligten Wechselrichtern garantieren. Darüber hinaus stellt sich heraus, dass der DAPI Regler bei geeigneter Auswahl der Droopkoeffizienten eine quadratische Funktion der Sekundärregelenergiekosten minimiert.

Acknowledgments

First of all, I wish to express my gratitude to my advisor at the University of California, Santa Barbara, Florian Dörfler. He has given me very valuable technical and methodological advice in my research. Besides, his continuous support and positive attitude have been a constant encouragement to me before, during and after the six months I spent in Santa Barbara. Working under his guidance has been a pleasure, a honor and a great learning process.

I also would like to thank Prof. Francesco Bullo very much, not only for the great financial support that made my stay possible and very pleasant, but also for his great advice and encouragement. I am also very thankful to everyone in Prof. Bullo's group for the friendly and serious working atmosphere. I would like to acknowledge especially John Simpon-Porco, with whom I had the pleasure to work and who never hesitated in helping me in different matters.

My stay in California could never have been such an unforgettable experience without the great people and good friends I met. I do not forget my mother, my family and my friends from all over the world, who were very supportive and gave me great advice in several occasions.

Finally, I wish to thank all the people at the University of Stuttgart who participated in teaching and educating me. My greatest thanks goes to Prof. Frank Allgöwer, who made this great experience possible and to my advisor at the Institute for Systems Theory and Automatic Control, University of Stuttgart, Mathias Bürger.

1 Introduction

1.1 Microgrids and Control

The electrical power grid has been undergoing some major structural changes in the last decade. These changes are mainly related to the emergence and penetration of competitive renewable energy technologies, especially photovoltaics and wind turbines. Both latter technologies feature some major differences from classical large fossil-fuel or nuclear power plants. They are characterized by strong fluctuations due to weather conditions, are often small units widely distributed in the lower voltage levels (Low voltage LV and Medium Voltage MV), and do not possess the inherent synchronization mechanism of coupled synchronous generators.

This continuous shift from centralized continuous power generation to distributed fluctuating power generation has been responsible for the emergence of several challenges, particularly regarding the stability of power systems. Thus, both the operation of the power grid and the analysis of its dynamics require new analysis tools and new control design concepts.

One of these concepts that has received increasing interest recently are the so-called *microgrids*. A microgrid is a local low-voltage electrical network connecting a set of heterogeneous loads, generation and storage units. It is able to be either coupled to a wide area synchronous grid or work in isolated and independent manner. Katiraei, Iravani and Lehn [18] identified the microgrid as a solution for stability problems subsequent to islanding events. This has been established by Peças Lopes, Moreira and Madureira in [24].

The electrical power output from renewables is very often not directly compatible with Alternate Current (AC) synchronous microgrids. Hence, it needs to be interfaced by power electronic devices, the *power inverters*, that transform heterogeneous electric power into AC power with a proper voltage frequency and ready to be injected into the synchronous AC electrical network.

Now, we consider microgrids as synchronous AC networks into which the entire AC power is injected through inverters; it becomes clear that all

important control operations are to be ensured through the control of the inverters network.

The main control objectives in a microgrid are

- ensuring balance between load demand and power injection,
- synchronizing the inverters frequencies to a rated value and stabilizing the voltages,
- sharing the load among the inverters in a fair manner (e.g. proportionally to their ratings).

Thereby, the following requirements are important for a practicable and robust operation of the microgrid.

- The communication complexity needs to be minimized in a way that allows a "plug-and-play"-like operation, that is, it should be possible to connect new inverters to the network without modifying the control structure or parameters.
- The control operation must be fast enough to cope with time-varying loads and fluctuating generation.

1.2 Literature review

The early work by Chandorkar, Divan and Adapa [8] transferred the concept of *conventional frequency- and voltage-droop control* from classical synchronous generators to parallel inverters in inductive networks. Lasseter introduced the microgrid idea in [21] and identified droop control as a way to ensure the main control objectives as well as a flexible plug-and-play operation and the minimization of communication needs. Similar results can be found in [5, 15, 22, 24, 25, 32].

Droop control being a proportional control law, it cannot avoid deviations from nominal values. As a way to regulate the micrgrid frequency to a nominal value, several papers [8, 16, 20] proposed to use the hierarchic control structure used in large-scale power networks and consisting basically in some *secondary* integral action subsequent to the *primary* proportional droop control. In [27] state feedback is combined with a decentralized LMI strategy to ensure stabilization and frequency regulation, while [2]

studies the performance of centralized and decentralized frequency-control algorithms based on integral action.

The recent work by Simpson-Porco, Dörfler, and Bullo [30] gives a novel analytic sufficient and necessary parametric condition for the existence of a unique and locally exponentially stable steady state in a lossless frequency-droop-controlled acyclic network with constant bus voltages. This condition was obtained following the observation of equivalence between droop-controlled lossless systems and a *generalized Kuramoto model* (see [10, 12] and the references therein for a survey of the Kuramoto synchronization theory for coupled oscillators). Simpson-Porco et al. [30] also give a selection of inverter parameters (droop coefficients and set points) that guarantee proportional load sharing among the inverters. Furthermore, they extend the primary droop-control by a secondary-control scheme, called the *distributed averaging PI (DAPI)* controller. This secondary control permits to dynamically regulate the network frequency to its nominal value while preserving the proportional power sharing and without time-scales separation. These results are foundational to this thesis and will be reviewed in Section 3.1.

Another relavant references for this thesis are [29] by Shafiee, Vasquez and Guerrero, as well as [1] by Andreasson et al.. Schafiee et al. present in [29] a secondary-control scheme based on all-to-all inverter frequency averaging. This work will be reviewed and revisited in Section 3.2. Andreasson et al. compare in [1] between a centralized and a decentralized control scheme that minimize the generation cost of control power in general electrical power systems.

Zhong points out in [35] some restrictions to the use of the conventional droop-control method in microgrids, mainly related to the important losses due to line resistances in low voltage networks. This problem is receiving increasing interest. Engler and Soultanis [13] propose the use of *opposite droops* as a substitute to conventional droop; in resistive LV grids, active power is related to voltage magnitudes and reactive power to voltage angles, while in inductive networks, active power is related to voltage angles and reactive power to voltage magnitudes. Liang et al. propose in [23] a modified droop-controller that enhances stability in lossy networks. Wang, Xia and Lemon [33] present sufficient conditions for voltage stability in a droop-controlled lossy microgrid. Schiffer et al. [28] establish the equivalence of the second-order dynamics of a synchronous generator and the dynamics a frequency-droop controlled inverter in a lossy network.

1.3 Contributions and Structure

In this work, we present and study two recent distributed secondary-control algorithms in microgrids and also introduce some related extensions within a nonlinear analysis framework. The contributions are fourfold. First, we present a nonlinear analysis of drooped-controlled inverters in a lossless microgrid equipped with a *centralized Averaging PI (CAPI)* secondary controller inspired by [29]. Second, we study the use of the DAPI controller from [30] to minimize a quadratic generation cost function. Third, we extend the nonlinear analysis of the DAPI- and CAPI-controlled systems to the lossy case. Finally, we investigate the possibility of reducing the communication complexity needed by the DAPI- and the CAPI-controller by restricting secondary-control actions to a subset of inverters.

The remainder of this work is organized as follows. In Chapter 2, we introduce the reader to some notations and definitions that are relevant for the study of secondary control in microgrids. We also present primary droop control and review the stability analysis from [30]. Chapter 3 deals with the secondary controllers DAPI and CAPI. Section 3.1 is a review of the DAPI control. Section 3.2 presents the CAPI controller and the analysis of the nonlinear dynamics of a CAPI-controlled microgrid. Section 3.3 proposes the DAPI controller as optimal controller. In Chapter 4, we extend the analysis of DAPI and CAPI control to lossy microgrids (Section 4.1) and to partial secondary control (Section 4.2).

Some of the results presented in this thesis have been submitted in the following article:

- H. Bouattour, J. W. Simpson-Porco, F. Dörfler and F. Bullo. Further Results on Distributed Secondary Control in Microgrids. In *IEEE Conf. on Decision and Control,* Florence, Italy, December 2013. Submitted.

2 Definitions and Problem Setup

2.1 Power Inverters and Droop Control

Most renewable energy sources that are connected to microgrids are not suitable for direct connection to a synchronous AC power system since they generate either incompatible Direct Current (DC) power (e.g. photovoltaics) or AC power with variable frequency (e.g. wind turbines). Therefore, power generated by renewables needs to be converted into AC power with the proper nominal frequency (e.g. 60 Hz for the North American power grid) before being injected into a synchronous AC microgrid. This task is performed by highly nonlinear power electronics devices called DC/AC (or AC/AC) converters, also known as power inverters or just *inverters*.

There are different types of inverters, depending among other things on the nature of the source supply (current or voltage source), on the nature of the output (current or voltage source) and on the electronic components (e.g. Thyristors, IGBT, MOSFET) [36]. For the purposes of this work, and as widely adopted in the microgrid literature, we will consider the class of voltage controlled *Voltage Source Inverters (VSI)* with purely sinusoidal voltage output. The switching transients, higher harmonics, and internal losses of the inverters are not relevant for the analysis of microgrid dynamics, so that we consider inverters to be ideal output voltage sources [24].

The amplitude of the VSI output as well as its frequency can be manipulated via pulse-width-modulation (PWM) techniques (a description of the relevant and widely-used sinusoidal PWM and further references to other PWM techniques can be found in [36]). Accordingly, it is possible through external control actions to set the amplitude and the angle velocity of the sinusoidal output voltage to be fed into the microgrid.

Further explanations of the internal physical composition and operation mode of inverters will not be addressed in this work and can be found in [14], [34] and [36].

High voltage networks are characterized by *inductive* power lines. This results in decoupling *active* power flow, controlled by the difference of bus angles, from *reactive* power flow, controlled by the difference of bus voltages.

Droop control is a technique based on this decoupling and widely used in the control of high-voltage large-scale power networks. *Frequency-droop* controls the active power output of a synchronous generator proportionally to the locally available measurement of the network AC frequency. The physical intuition behind this idea is clear for a synchronous generator since there is an inverse-proportional relationship between the electrical active power output and the frequency of the rotating mass [19].

Chandorkar et al. introduces in [8] conventional frequency-droop control for an inverter with inductive output impedance. Droop control emulates the behavior of a synchronous generator and specifies an instantaneous change in the frequency ω_i of the voltage signal at an inverter i according to the frequency-droop law

$$\omega_i = \omega^* - m_i(P_{e,i} - P_i^*)\,, \tag{2.1}$$

where ω^* is the rated frequency, $P_{e,i}$ is the active electrical power injection of inverter i and P_i^* is the nominal active power injection of inverter i when operated at the rated frequency. The parameter $m_i > 0$ is referred to as the droop coefficient.

2.2 Notation and Geometric Definitions

The following section introduces the reader to the notation used throughout this thesis as well as to some important geometric definitions.

Notation

- Given a finite set $\mathcal{V}$, let $|\mathcal{V}|$ denote its cardinality.
- Given an n-tuple $(x_1, \ldots, x_n)$, let $x \in \mathbb{R}^n$ be the associated vector.
- Given an index set $\mathcal{I}$ and a real valued 1-dimensional array $\{x_1, \ldots, x_{|\mathcal{I}|}\}$, let $\mathrm{diag}(\{x_i\}_{i\in\mathcal{I}}) \in \mathbb{R}^{|\mathcal{I}|\times|\mathcal{I}|}$ be the associated diagonal matrix.
- We denote the $n \times n$ identity matrix by I_n. Let $\mathbf{1}_n$ and $\mathbf{0}_n$ be the n-dimensional vectors of all ones and all zeros. We will drop the subscripts from I_n, $\mathbf{1}_n$ and $\mathbf{0}_n$ when the dimensions are clear from context.

- Let $\mathcal{V} = \{1, \dots, n\}$ be a finite partitioned set $\mathcal{V} = \mathcal{V}_L \cup \mathcal{V}_I$. For simplicity of notation, let $|\mathcal{V}_L| = n_L$ and $|\mathcal{V}_I| = n_I$. A vector $x \in \mathbb{R}^n$ inherits the partitioning as $x = (x_L, x_I)$, where $x_L \in \mathbb{R}^{n_L}$ and $x_I \in \mathbb{R}^{n_I}$.
- For $x \in \mathbb{R}^n$, let $\mathbf{sin}(x) \triangleq (\sin(x_1), \dots, \sin(x_n))^T \in \mathbb{R}^n$.

Geometry on the n-torus:

- The set $\mathbb{S}^1$ denotes the *unit circle*, an *angle* is a point $\theta_i \in \mathbb{S}^1$, and an *arc* is a connected subset of $\mathbb{S}^1$.
- With a slight abuse of notation, let $|\theta_1 - \theta_2|$ denote the *geodesic distance* between two angles $\theta_1, \theta_2 \in \mathbb{S}^1$.
- The *n-torus* $\mathbb{T}^n = \mathbb{S}^1 \times \cdots \times \mathbb{S}^1$ is the Cartesian product of n unit circles.
- For $\gamma \in [0, \pi/2[$ and a given graph $G(\mathcal{V}, \mathcal{E}, \cdot)$, let

$$\Delta_G(\gamma) = \{\theta \in \mathbb{T}^{|\mathcal{V}|} : \max_{\{i,j\} \in \mathcal{E}} |\theta_i - \theta_j| \leq \gamma\}$$

  be the closed set of angle arrays $\theta = (\theta_1, \dots, \theta_n)$ with neighboring angles θ_i and θ_j, $\{i,j\} \in \mathcal{E}$ no further than γ apart.

2.3 Algebraic Graph Theory

We denote by $G(\mathcal{V}, \mathcal{E}, A)$ an undirected and weighted graph, where $\mathcal{V} = \{1, \dots, n\}$ is the set of nodes, $\mathcal{E} \subseteq \mathcal{V} \times \mathcal{V}$ is the set of edges, and $A \in \mathbb{R}^{n \times n}$ is the *adjacency matrix*.

If a number $\ell \in \{1, \dots, |\mathcal{E}|\}$ and an arbitrary direction are assigned to each edge $\{i,j\} \in \mathcal{E}$, the *node-edge incidence matrix* $B \in \mathbb{R}^{n \times |\mathcal{E}|}$ is defined component-wise as $B_{k\ell} = 1$ if node k is the sink node of edge ℓ and as $B_{k\ell} = -1$ if node k is the source node of edge ℓ, with all other elements being zero. For $x \in \mathbb{R}^n$, $B^T x \in \mathbb{R}^{|\mathcal{E}|}$ is the vector with components $x_i - x_j$, with $\{i,j\} \in \mathcal{E}$.

The *Laplacian matrix* $L \in \mathbb{R}^{n \times n}$ is defined by $L_{ij} = \begin{cases} -a_{ij} & \text{for } i \neq j \\ \sum_{j=1, j \neq i}^{n} a_{ij} & \text{for } i = j \end{cases}$, a_{ij} being the weight of the edge between nodes i and j. L is positive semidef-

inite and satisfies the identity $L = B\mathcal{A}B^T$ with $\mathcal{A} \triangleq \text{diag}(\{a_{ij}\}_{\{i,j\}\in\mathcal{E}})$ being the diagonal matrix of edge weights.

If the graph is connected, then $\ker(B^T) = \ker(L) = \text{span}(\mathbf{1}_n)$, and $\ker(B) = \emptyset$ for *acyclic* graphs. In the case of an acyclic graph, for every $x \in \mathbb{R}^n$ with $\sum_{i\in\mathcal{V}} x_i = 0$, there exists a unique $\xi \in \mathbb{R}^{|\mathcal{E}|}$ satisfying Kirchoff's Current Law (KCL) $x = B\xi$ [6, 9]. The vector x is interpreted as nodal injections, with ξ being the associated flows along edges.

We denote by $B^\dagger \triangleq (B^TB)^{-1}B^T$ the left pseudoinverse of B.

2.4 Active Power Flow in AC networks

Consider a synchronous AC electrical power network with a set $\mathcal{V} = \{1,\dots,n\}$ of nodes and a set $\mathcal{E} \in \mathcal{V}\times\mathcal{V}$ of power lines. The active power flow $P_{e,i\to j} \in \mathbb{R}$ from node i to node j is given by [19] as

$$P_{e,i\to j} = E_iE_j\left|Y_{ij}\right| sin(\theta_i - \theta_j - \phi_{ij}), \tag{2.2}$$

the reactive power flow $Q_{e,i\to j} \in \mathbb{R}$ from node i to node j as

$$Q_{e,i\to j} = E_iE_j\left|Y_{ij}\right| cos(\theta_i - \theta_j - \phi_{ij}), \tag{2.3}$$

where $E \in \mathbb{R}^n_{\geq 0}$ is the vector of voltage magnitudes at the nodes, $Y \in \mathbb{C}^{n\times n}$ is the *admittance matrix* and $\theta \in \mathbb{T}^n$ represents the voltage angles at the nodes. For all $\{i,j\} \in \mathcal{E}$, the admittance phase is defined as $\phi_{ij} \triangleq -\arctan(\mathcal{G}_{ij}/\mathcal{B}_{ij})$ with $\mathcal{G}_{ij} = \Re(Y_{ij})$ being the line *conductance*, and $\mathcal{B}_{ij} = \Im(Y_{ij})$ the line *susceptance*. Note that the power flow $P_{e,i\to j}$ is lossless if $\mathcal{G}_{ij} = 0$.

The active electrical power $P_{e,i} \in \mathbb{R}$ injected into the network at node $i \in \{1,\dots,n\}$ is then given as

$$P_{e,i}(\theta) = \sum_{j=1}^{n} E_iE_j\left|Y_{ij}\right| \sin(\theta_i - \theta_j - \phi_{ij}), \tag{2.4}$$

where we assume the voltage magnitudes E_i, $i \in \{1,\dots,n\}$, to be constant parameters. This assumption can also be relaxed to unknown and strictly positive parameters, see [30, Corollary 5].

Remark 1. ***Power flow is rotationally invariant.***
Observe that the active power flow $P_{i\to j}$ and hence the active power injection $P_{e,i}(\theta)$ are rotationally invariant, *that is, by rotating the angles θ_i and θ_j by the same angle in the same direction, $P_{i\to j}$ and $P_{e,i}(\theta)$ do not change.* □

Remark 2. ***Lossless power flow is symmetric.***
Under assumption of lossless power flow, i.e., there are no conductances in the network $\mathcal{G}_{ij} = 0$ *and hence* $\phi_{ij} = 0$ *for all* $\{i,j\} \in \mathcal{E}$*, the electrical power flow is symmetric, that is* $P_{\mathrm{e},i \to j} = P_{\mathrm{e},j \to i}$ *. Note that the sum of the symmetric power flow over all nodes is zero:* $\mathbf{1}^T P_{\mathrm{e}} = 0$. □

2.5 Droop-Controlled Microgrid

For our purposes, a microgrid is a *standalone* synchronous AC system in which the entire AC power is injected into the network through inverters. A standalone microgrid is operated isolated from the rest of the electrical power grid, which can be a design choice or can happen as a consequence to some disturbances. The inverters are operated as ideal voltage sources.

By neglecting eventual control of the line susceptances, we reduce the control of a microgrid to the control of a network of inverters. Accordingly, power balance, stability, and load sharing in the microgrid have to be ensured through the control of the inverters.

Our microgrid setup consists of n_I Voltage Source Inverters (VSI) with ratings $\overline{P}_i \in \mathbb{R}_{\geq 0}$ and n_L frequency-independent loads connected through a synchronous AC electrical network. We model it as an undirected and weighted graph $G(\mathcal{V},\mathcal{E},A)$, where the partitioned set of nodes $\mathcal{V} = \{\mathcal{V}_L,\mathcal{V}_I\} = \{1,\dots,n\}$ corresponds to the n_L loads and n_I inverters in the electrical network, $\mathcal{E} \in \mathcal{V} \times \mathcal{V}$ represents the set of power lines and the entries of the weighted adjacency matrix $A \in \mathbb{R}^{n \times n}$ are $a_{ij} = E_i E_j \left|Y_{ij}\right| > 0$ if $\{i,j\} \in \mathcal{E}$ and $a_{ij} = 0$ otherwise.

For the seek of simplicity, we adopt the physically reasonable and widely adopted assumption of decoupled active power flow and reactive power, see [19]. Active power flow is controlled by the difference of bus voltage angles via a frequency-droop controller while the bus voltages are assumed to be constant and hence the reactive power flow is almost constant.

Each inverter is equipped with a *primary* frequency-droop controller (2.1) and possibly a *secondary* controller that changes the set point P^* of the power output. We choose to describe the system in relative coordinates and set the time derivative of the voltage angle at inverter i as $\dot{\theta}_i = \omega^* - \omega_i$. The rated frequency is now 0 Hz instead of 60 Hz (in the North American Power Grid). We also introduce the *inverse droop coefficients* as $D_i = 1/m_i$ and will refer to them simply and without any loss of generality as *droop coefficients*.

All loads are assumed to be frequency-independent, that is the voltage angles at the load nodes are constant. The closed-loop dynamics of the *droop-controlled* microgrid are then given by the differential-algebraic system

$$0 = P_i^* - P_{\mathrm{e},i}(\theta)\,, \quad i \in \mathcal{V}_L\,. \tag{2.5a}$$

$$D_i\dot{\theta}_i = P_i^* - P_{\mathrm{e},i}(\theta) + u_i(t), \quad i \in \mathcal{V}_I\,, \tag{2.5b}$$

where $u_i : \mathbb{R}_{\geq 0} \to \mathbb{R}$ is the *secondary control input* at node i. From this point on, we will refer to the closed-loop system (2.5b) without secondary control input $u_i = 0$ for all $i \in \mathcal{V}_I$ as the *primary-controlled system*. In presence of a nonzero control input, we refer to (2.5b) as the *secondary-controlled system*.

The synchronization of the inverters output frequencies is one of the main control objectives in a microgrid. We define it as follows.

Definition 1. ***Synchronization:***
A trajectory $\theta : \mathbb{R}_{\geq 0} \to \mathbb{T}^n$ *is* synchronized *if the following statements hold*

(a) There exists a constant $\omega_{\mathrm{sync}} \in \mathbb{R}$ *such that* $\dot{\theta} = \omega_{\mathrm{sync}}\mathbf{1}$ *for all* $t \geq 0$.

(b) There exists a $\gamma \in [0, \pi/2[$ *such that* $\theta(t) \in \Delta(\gamma)$ *for all* $t \geq 0$.

First, consider the primary-controlled system. If there exists a synchronized trajectory $\theta^* : \mathbb{R}_{\geq 0} \to \mathbb{R}$ for which holds that $\dot{\theta}_i^*(t) = \omega_{\mathrm{sync}}\ \forall t \geq 0$, then by summing up over the equations (2.5a)-(2.5b), we obtain the synchronization frequency as:

$$\omega_{\mathrm{sync}} = \frac{-P_L + \sum\limits_{i\in\mathcal{V}_l} P_i^* + \sum\limits_{i\in\mathcal{V}} P_{\mathrm{e},i}(\theta^*)}{\sum\limits_{i\in\mathcal{V}_l} D_i} = \frac{\sum\limits_{i\in\mathcal{V}} P_i^* + \sum\limits_{i\in\mathcal{V}} P_{\mathrm{e},i}(\theta^*)}{\sum\limits_{i\in\mathcal{V}_l} D_i}\,, \tag{2.6}$$

where $P_L = \sum_{i\in\mathcal{V}_L} P_i^* \in \mathbb{R}_{\geq 0}$ is the total load. Note that the synchronization frequency is not zero in the general case. In the lossless case, the power flows sum up to zero and we call the synchronization frequency *scaled power imbalance* $\omega_{\mathrm{avg}} \triangleq \frac{\sum_{i\in\mathcal{V}} P_i^*}{\sum_{i\in\mathcal{V}_l} D_i}$. [30]

We associate to the primary-controlled system (2.5a)-(2.5b) an auxiliary system that we define as

$$0 = \widetilde{P}_i - P_{\mathrm{e},i}(\theta)\,, \quad i \in \mathcal{V}_L\,, \tag{2.7a}$$

$$D_i\dot{\theta}_i = \widetilde{P}_i - P_{\mathrm{e},i}(\theta), \quad i \in \mathcal{V}_I\,, \tag{2.7b}$$

where $\widetilde{P}_i = P_i^*$ for all $i \in \mathcal{V}_L$ and $\widetilde{P}_i = P_i^* - D_i\omega_{\text{avg}}$ for all $i \in \mathcal{V}_I$. Since $\mathbf{1}^T\widetilde{P} = 0$, system (2.7) features the property that $\dot{\widetilde{\omega}}_{\text{avg}} = 0$. Hence, a synchronized solution of (2.5) is an equilibrium of (2.7).

The recent work by Simpson-Porco et al. [30] is foundational for this thesis. It presents a nonlinear analysis of the angle stability and power sharing properties in an inductive microgrid. Particularly in the case of a lossless acyclic network with constant bus voltages, it gives necessary and sufficient conditions for the existence and uniqueness of a frequency-synchronized solution to the differential algebraic system (2.5).

Before stating the main result from [30], observe that synchronized solutions to the closed-loop system (2.5) live on synchronization manifolds, which are defined as follows.

Definition 2. ***Synchronization Manifold:***
Since the power flow is rotationally invariant, if $\theta \in \Delta_G(\gamma) \subset \mathbb{T}^n$ for some $\gamma \in [0,\pi/2[$ is a synchronized solution of the closed-loop system (2.5), then every $\theta + s\mathbf{1}_n$ with $s \in [0,2\pi]$ lives also in $\Delta_G(\gamma)$ and is a synchronized solution of (2.5). The set $\mathcal{R}_\theta \triangleq \{\theta + s\mathbf{1}_n \mid s \in [0,2\pi]\}$ is called the synchronization manifold.

These concepts allow us to state the following result [30, Theorem 2]:

Theorem 2.5.1. ***Existence and Stability of Synchronized Solution.***
Consider the primary-controlled system (2.5) defined on an acyclic lossless network with node-edge incidence matrix B. Define the scaled power imbalance $\omega_{\text{avg}} \triangleq \dfrac{\sum_{i\in\mathcal{V}} P_i^*}{\sum_{i\in\mathcal{V}_I} D_i}$ and let $\xi \in \mathbb{R}^{|\mathcal{E}|}$ be the unique vector of edge power flows satisfying KCL, given by $\xi = B^\dagger(P^* - \omega_{\text{avg}}D\mathbf{1})$, with $D = \text{diag}(\mathbf{0}_{n_L}, \{D_i\}_{i\in\mathcal{V}_I})$. The following two statements are equivalent:

(i) ***Synchronization:*** *There exists an arc length $\gamma \in [0,\pi/2[$ such that the closed-loop system (2.5) possesses a locally exponentially stable and unique[†] synchronized solution $t \mapsto \theta^*(t) \in \Delta_G(\gamma)$ for all $t \geq 0$; and*

(ii) ***Flow Feasibility:*** *The power flow is feasible, i.e.,*

$$\Gamma \triangleq \|\mathcal{A}^{-1}\xi\|_\infty < 1. \tag{2.8}$$

[†]Modulo the rotational symmetry inherent in the model.

If the equivalent statements (i) and (ii) hold true, then the quantities $\Gamma \in [0,1[$ *and* $\gamma \in [0,\pi/2[$ *are related uniquely via* $\Gamma = \sin(\gamma)$*, the synchronized solution satisfies* $\theta^*(t) = \theta_0 + \left(\omega_{\text{sync}} t \mathbf{1}_n\right) \pmod{2\pi}$ *for some* $\theta_0 \in \Delta_G(\gamma)$*, where* $\omega_{\text{sync}} = \omega_{\text{avg}}$*, and the synchronized angular differences satisfy* $\mathbf{sin}(B^T\theta^*) = \mathcal{A}\xi$.

Note that the power injection of each inverter is constrained by its rating, that is, $P_{e,i} \in [0,\overline{P}_i]$ for each inverter $i \in \mathcal{V}_I$. Yet we do not know how to select the droop coefficients D_i and the set points P_i^* of the inverters in order to satisfy these actuation constraints. Consider the following proportional selection of the inverters parameters D_i and P_i^*:

Definition 3. ***Proportional inverter parameters***
The parameters of the inverters, the droop coefficients and the set points, are selected proportionally *if for all* $i, j \in \mathcal{V}_I$

(a) $\dfrac{P_i^*}{D_i} = \dfrac{P_j^*}{D_j}$ *and (b)* $\dfrac{P_i^*}{\overline{P}_i} = \dfrac{P_j^*}{\overline{P}_j}$.

Simpson-Porco et al. show in the following theorem [30, Theorem 7] that a proportional selection of the inverter parameters after Definition 3 leads to an equivalence between the satisfaction of the actuation constraints and the serviceability of the load, and guarantees proportional power sharing.

Theorem 2.5.2. ***Power Flow Constraints and Power Sharing.***
Consider a synchronized solution of the primary-controlled lossless network of load and inverters (2.5) and let the inverter parameters be selected proportionally. The following two statements are equivalent:

(i) **Injection Constraints:** $0 \leq P_{e,i} \leq \overline{P}_i,\ \forall i \in \mathcal{V}_I$*; and*

(ii) **Load Constraints:** $-\sum_{j\in\mathcal{V}_I} \overline{P}_j \leq P_L \leq 0$.

Moreover, the inverters share the total load P_L *proportionally according to their power ratings, that is,* $P_{e,i}/\overline{P}_i = P_{e,j}/\overline{P}_j$*, for each* $i \in \mathcal{V}_I$.

2.6 General Simulation Setup

Throughout this work, we will support and illustrate our analytic results with a few simulations. For this aim, we consider two inverters operating in parallel, supplying a time-varying load and connected through lossy power lines. The frequency of each inverter is controlled via droop control (2.5b). The simulation time is 15 seconds. The active power demand is constant

over the first five seconds, doubles then remains constant over the second five seconds and finally returns to its initial value in the last five seconds.

The verification of the stability condition stated in Theorem 2.5.1 is dependent on the terms $a_{ij} = E_i E_j \left|Y_{ij}\right|$, $\{i,j\} \in \mathcal{E}$. While the analysis assumes constant voltage magnitudes and constant susceptances, in realistic power systems both are dynamically regulated by further controllers. On the other hand, the droop controller (2.5) features some robustness to variable voltage and susceptances magnitudes, as shown in [30, Corollary: 5]. In order to confirm the robustness of the controllers that will be analyzed in this work, we introduce voltage control and use lossy lines in our simulation scenarios.

The voltage magnitude at each inverter is controlled via the *quadratic voltage-droop method* [31]

$$\tau_i \dot{E}_i = -C_i E_i (E_i - E_i^*) - Q_{e,i}\,, \quad i \in \mathcal{V}_I\,, \quad i \in \{1,2\},$$

where $E_i^* > 0$ is the nominal voltage magnitude, $C_i > 0$ and $\tau_i > 0$ are the proportional and integral quadratic voltage-droop coefficients, and $Q_{e,i} \in \mathbb{R}$ is the reactive power injection [19].

The general simulation parameters are specified in Table 2.1. We will use these parameters for most the simulations throughout this work. Whereas our choice of the parameter values will lead to satisfying transients, its optimization is not subject of this work. Note also that the choice of a load that is small relatively to the inverter set points is motivated by the presence of losses in the network, which need to be compensated by a higher power injection from the nodes. This will be the object of detailed analysis in Subsection 4.2.2.

The first simulation scenario (see Figure 2.1) illustrates the stability and power sharing properties of the primary-controlled system (2.5). On the one hand, observe that the frequencies are synchronized in steady state, that the power sharing property holds also in steady state. On the other hand, note that the synchronization frequency is different from the rated frequency 60 Hz. This motivates the implementation of some integral secondary control action, which would eliminate the frequency deviation in steady state.

Table 2.1: General parameter values.

Parameter	Symbol	Value
Nom. Frequency	$\omega^*/2\pi$	60 Hz
Nom. Voltages	E_i^*	$[120, 122]$ V
Output/Line Induc.	L_i	$[0.7, 0.5]$ mH
Output/Line Resist.	R_i	$[0.14, 0.1]\,\Omega$
Inv. Ratings (P)	$P_i^* = \overline{P}_i$	$[6, 9]$ kW
Load (P)	$P_0^*(t)$	$P_0^* \in \{-2.5, -5\}$kW
Load (Q)	$Q_0^*(t)$	$Q_0^* \in \{-.5, -1\}$kvar
ω–Droop Coeff.	D_i	$[4, 6] \times 10^3$ W $\cdot$ s
Quadratic E–Droop Coeff.	C_i	$[1, 1] \times 10^3$ S
Quadratic E–Droop Int. Coeff.	τ_i	$[5, 5]$ $\frac{\text{Var}}{\text{V}} \cdot$ s

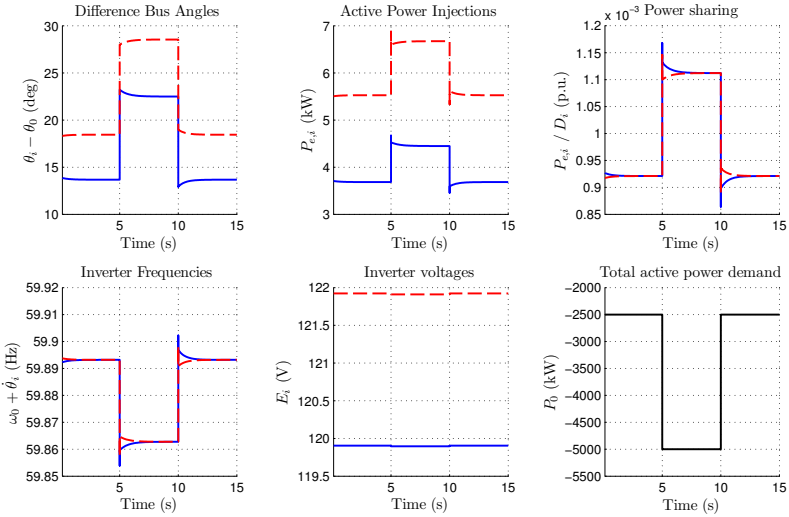

Figure 2.1: Primary-controlled microgrid consisting of two parallel inverters supplying a load, which changes at $t \in \{5s, 10s\}$.

3 Secondary Control Strategies in a Microgrid

As we have seen in Theorem 2.5.1 and in Figure 2.1, in synchronized steady state, the primary-controlled system (2.5) features generally a frequency deviation $\omega_{\text{avg}} \neq 0$. Thus, it is necessary to extend the primary droop controller by some secondary integral control action able to eliminate these deviations. At the same time, this integral control action should not lead to some arbitrary power flows in steady state, but rather conserve the proportional power sharing property of droop control or alternatively optimize some cost function.

First, observe that the synchronization frequency for the auxiliary system (2.7) is $\overline{\omega}_{\text{avg}} = 0$. The dynamics of this auxiliary system correspond to the dynamics of the original system (2.5) in a rotating frame with the frequency ω_{avg}. Intuitively, one approach would be to make the secondary control input u transform the system into this rotating frame by setting $u_i = D_i \omega_{\text{avg}}$ for each $i \in \mathcal{V}_I$.

Unfortunately, ω_{avg} is not immediately available locally at each inverter, which makes the design of a secondary-control strategy a particularly challenging problem.

On the one hand, a computation of ω_{avg} as defined by (2.6) requires the knowledge of all droop coefficients, of all power set points and of the possibly time-varying loads. This computation does not feature any robustness against the presence of losses in the network. Therefore, it is practically not relevant.

On the other hand, a totally decentralized implementation, as described by Chandorkar et al. [8], uses $\dot{\theta}_i$ as an approximation of ω_{avg} at each node $i \in \mathcal{V}_I$. Hence, it requires a separation of time scales between fast primary control and slow secondary control. In the fast time scale, the primary control ensures the synchronization of all voltage angles. In the slow time scale, the secondary control uses the synchronization frequency ω_{avg} (which is by then available at each node) to change the set point of the inverter and eliminate the frequency deviation. This slow secondary control is not

able to dynamically regulate the frequency to the rated value in presence of time-varying load.

In order to avoid such a control strategy requiring a time scale separation, a dynamic secondary control strategy is preferred which assures the convergence of the input u_i to $D_i\omega_{\text{avg}}$ while the primary control ensures frequency-synchronization at the same time.

In this section, we will present two secondary-control algorithms and discuss their stability and power sharing properties.

3.1 Distributed Averaging PI Control

The work by Simpson-Porco et al. [30] presents a distributed secondary control algorithm for frequency control. The controller is given by:

$$u_i = -p_i \ , \ k_i \dot{p}_i = D_i \dot{\theta}_i - \sum_{j \in \mathcal{V}_I} L_{c,ij} \left(\frac{p_i}{D_i} - \frac{p_j}{D_j} \right) . \tag{3.1}$$

Here, $L_c \in \mathbb{R}^{n_I \times n_I}$ is the symmetric Laplacian matrix of a connected communication graph G_c between the inverters $\{1, \ldots, n_I\}$ (see Figure 3.1). For each $i \in \mathcal{V}_I$, $p_i \in \mathbb{R}$ is an auxiliary power variable and $k_i > 0$ is the control gain.

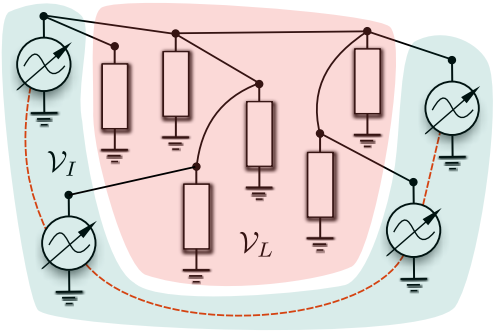

Figure 3.1: Schematic of secondary control. The red dotted line represents a communication link [30].

The resulting closed-loop system is then given by

$$0 = P_i^* - P_{\mathrm{e},i}(\theta)\,, \qquad i \in \mathcal{V}_L\,, \tag{3.2a}$$

$$D_i\dot{\theta}_i = P_i^* - p_i - P_{\mathrm{e},i}(\theta)\,, \qquad i \in \mathcal{V}_I\,, \tag{3.2b}$$

$$k_i\dot{p}_i = D_i\dot{\theta}_i - \sum_{j\in\mathcal{V}_I} L_{\mathrm{c},ij}\left(\frac{p_i}{D_i} - \frac{p_j}{D_j}\right), \qquad i \in \mathcal{V}_I\,. \tag{3.2c}$$

The controller (3.1) consists of a decentralized proportional-integral part $D_i\dot{\theta}_i$ and of the consensus term $\sum_{j\in\mathcal{V}_I} L_{\mathrm{c},ij}(p_i/D_i - p_j/D_j)$. The controller transforms the system (2.5) into the auxiliary system (2.7). Besides of dynamically regulating the system frequency in presence of time-varying loads, this controller, named *Distributed Averaging PI (DAPI) controller*, has the particular feature of preserving the power sharing property of primary control obtained by selecting the inverter parameters as shown in Definition 3.

In the following, we analyze the stability and the power sharing properties of this control strategy. To begin, we make sure that synchronized solutions of the DAPI-controlled system are necessarily equilibria of (3.2).

Lemma 3.1.1. ***Synchronization Frequency is Zero.***
If the frequencies of the inverters in the DAPI-controlled system (3.2) are synchronized, then the synchronization frequency is zero.

Proof. Assume there exists a solution $(\bar{\theta},\bar{p}) \in \Delta_G(\gamma) \times \mathbb{R}^{n_I}$ for the system (3.2) such that the trajectory $\bar{\theta} : \mathbb{R}_{\geq 0} \to \Delta_G(\gamma)$ is synchronized with $\dot{\bar{\theta}} = \overline{\omega}_{\mathrm{sync}}\mathbf{1} \in \mathbb{R}^{n_I}$ and the secondary control input $\bar{p} : \mathbb{R}_{\geq 0} \to \mathbb{R}^{n_I}$ is a time-varying function.

Equation (3.2b) becomes $D_i\overline{\omega}_{\mathrm{sync}} = P_i^* - \bar{p}_i - P_{\mathrm{e},i}(\bar{\theta})$ for all $i \in \mathcal{V}_I$. The terms $D_i\overline{\omega}_{\mathrm{sync}}$ and P_i^* are constant for each $i \in \mathcal{V}_I$. Note that also the power flow $P_{\mathrm{e},i}(\bar{\theta}) = \sum_{j=1}^{n} E_iE_j\left|Y_{ij}\right|\sin(\bar{\theta}_i - \bar{\theta}_j - \phi_{ij})$ is constant for each $i \in \mathcal{V}_I$ for synchronized $\bar{\theta}$ since $\dot{\bar{\theta}}_i - \dot{\bar{\theta}}_j = \overline{\omega}_{\mathrm{sync}} - \overline{\omega}_{\mathrm{sync}} = 0$ for all $i,j \in \mathcal{V}_I$. Therefore, also $\bar{p}_i$ is constant for each $i \in \mathcal{V}_I$ in synchronized state.

The row sum of the symmetric Laplacian L_{c} is zero. Therefore, by summing up the equations (3.2c) in steady state, we get $0 = \sum_{i\in\mathcal{V}_I} k_i\dot{\bar{p}}_i = \sum_{i\in\mathcal{V}_I} D_i\overline{\omega}_{\mathrm{sync}}$. Since $D_i > 0$ for all $i \in \mathcal{V}_I$, $\overline{\omega}_{\mathrm{sync}}$ must be zero. □

The following result gives a necessary and sufficient parametric condition for the local existence, uniqueness (modulo rotational symmetry) and exponential stability of an equilibrium of the DAPI-controlled system (3.2)

for a lossless acyclic network [30, Theorem: 8]. It also states that the DAPI controller preserves the proportional power sharing.

Theorem 3.1.2. ***Stability of DAPI-Controlled Network.***
Consider a lossless acyclic network of droop-controlled inverters and loads in which the inverters can communicate through the weighted graph G_c, as described by the closed-loop system (3.2) with parameters $k_i > 0$, $P_i^* \in [0, \overline{P}_i]$, and $D_i > 0$ for $i \in \mathcal{V}_I$, and connected communication Laplacian $L_c \in \mathbb{R}^{n_I \times n_I}$. The following two statements are equivalent:

(i) ***Stability of Droop Controller:*** *The droop control stability condition (2.8) holds; and*

(ii) ***Stability of DAPI Controller:*** *There exists an arc length $\gamma \in [0, \pi/2[$ such that the system (3.2) possesses a locally exponentially stable and unique[†] equilibrium $(\theta^*, p^*) \in \Delta_G(\gamma) \times \mathbb{R}^{n_I}$.*

If the equivalent statements (i) and (ii) hold true, then θ^* lives on the same synchronization manifold as the solution from Theorem 2.5.1 (ii), and $p_i^* = D_i \omega_{\text{avg}}$ for $i \in \mathcal{V}_I$. Moreover, if the droop coefficients are selected proportionally, then the DAPI controller (3.1) preserves the proportional power sharing property of the primary droop controller.

In the following simulation scenario, we use the general parameters from Table 2.1 and the DAPI parameters given by Table 3.1, and we illustrate the properties of the DAPI controller (3.1). The results are shown in Figure 3.2. Observe that the frequencies of both inverters return to the rated frequency quickly after the change of load and that the power sharing property is recovered in steady state.

Table 3.1: Specific parameter values for the DAPI controller.

Parameter	Symbol	Value
Sec. Droop Coeff.	k_i	10^{-6} s
Comm. Graph	G_{comm}	Two nodes, one edge
Comm. Laplacian	L_c	$(10^4 \text{ Ws}) \cdot \begin{bmatrix} 1 & -1 \\ -1 & 1 \end{bmatrix}$

[†]Modulo the rotational symmetry inherent in the model.

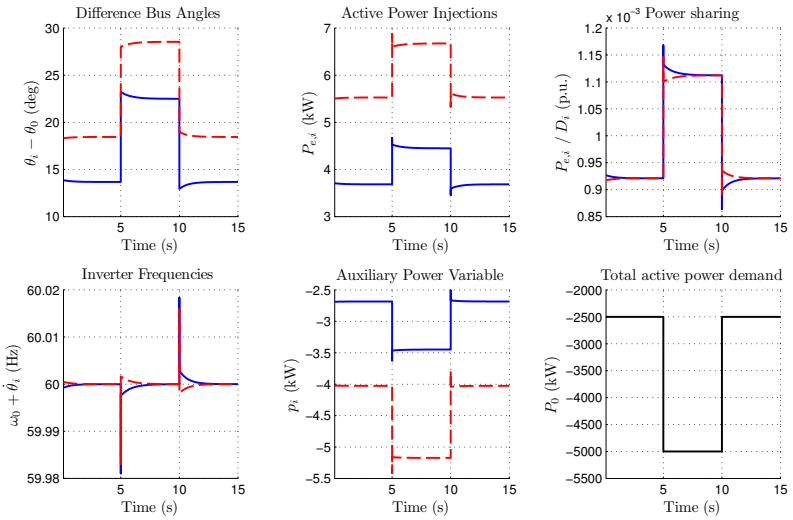

Figure 3.2: DAPI-controlled microgrid consisting of two parallel inverters supplying a load, which changes at $t \in \{5s, 10s\}$.

3.2 Centralized Averaging PI Control

Another secondary distributed PI controller has been presented by Shaffie et al. in [29]. The proposed secondary-control input $u_i(t)$ to the dynamics (2.5) is given by an integral feedback[‡] of the *weighted average frequency*[§] among the inverters:

$$u_i(t) = -p_i \ , \ k_i \dot{p}_i = \frac{\sum_{j \in \mathcal{V}_l} D_j \dot{\theta}_j}{\sum_{j \in \mathcal{V}_l} D_j} \ , \tag{3.3}$$

[‡] The controller proposed in [29] also contains a proportional feedback of the average frequency. We found that such a proportional feedback destroys the desired proportional power sharing, unless the gains are carefully tuned. For these reasons and since the resulting closed loop is hardly amenable to an analytic investigation, we omit the proportional feedback channel here.

[§] The controller in [29] contains a true arithmetic average with all $D_i = 1$ in (3.3). Since the synchronization frequency (2.6) is obtained by a weighted average, we found the choice (3.3) more appealing and intuitive. Simulation studies suggest that any convex combination of the inverter frequencies yields identical results.

Here, $p_i \in \mathbb{R}$ is again an auxiliary power variable and $k_i > 0$ is a gain, for each $i \in \mathcal{V}_I$.

A simulation using the general parameters from Table 2.1 and the controller parameters given by Table 3.2 shows that, while the frequencies are regulated, the proportional power sharing is destroyed (see Figure 3.3).

Table 3.2: Specific parameter values for controller (3.3)-(3.4).

Parameter	Symbol	Value
Sec. Droop Coeff.	k_i	10^{-6} s

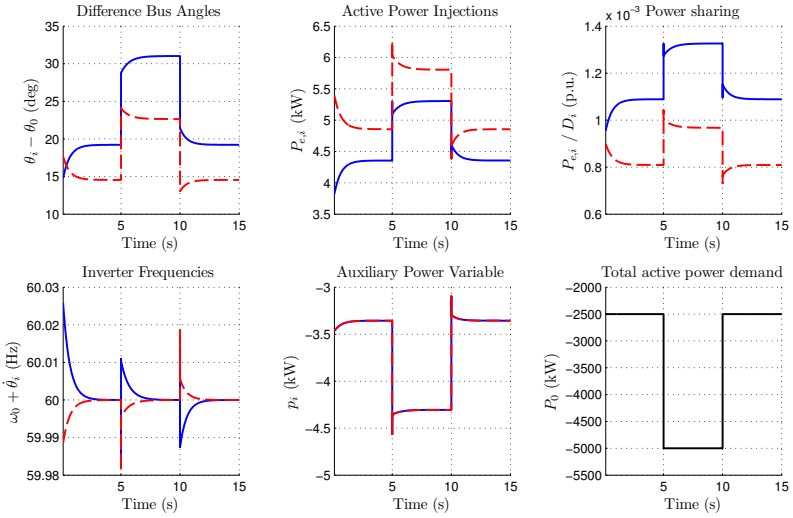

Figure 3.3: A microgrid consisting of two parallel inverters supplying a load, which changes at $t \in \{5s, 10s\}$, controlled by the controller (3.5).

It turns out, that a careful choice of the secondary-controller parameters can lead to the preserving of power sharing. In the following, we suggest the choice

$$k_i = k/D_i\,, \quad i \in \mathcal{V}_I\,. \tag{3.4}$$

where $k > 0$ is constant. That is, the integral channels have the time-constants *inverse* to the proportional droop control channels (2.5b). In this case, the closed loop is given by

$$0 = P_i^* - P_{\mathrm{e},i}(\theta)\,, \qquad i \in \mathcal{V}_L\,, \tag{3.5a}$$

$$D_i\dot{\theta}_i = P_i^* - P_{\mathrm{e},i}(\theta) - p_i\,, \qquad i \in \mathcal{V}_I\,, \tag{3.5b}$$

$$k\frac{\dot{p}_i}{D_i} = \frac{\sum_{j\in\mathcal{V}_I} D_j\dot{\theta}_j}{\sum_{j\in\mathcal{V}_I} D_j}\,, \qquad i \in \mathcal{V}_I\,. \tag{3.5c}$$

By changing coordinates $q_i = p_i/D_i - \omega_{\mathrm{avg}}$ for $i \in \mathcal{V}_I$ and observing that $k\dot{q}_i = \dfrac{\sum_{j\in\mathcal{V}_I} D_j\dot{\theta}_j}{\sum_{j\in\mathcal{V}_I} D_j}$ is identical for all $i \in \mathcal{V}_I$, we can rewrite the closed-loop equations (3.5) as

$$0 = \widetilde{P}_i - P_{\mathrm{e},i}(\theta)\,, \qquad i \in \mathcal{V}_L\,, \tag{3.6a}$$

$$D_i\dot{\theta}_i = \widetilde{P}_i - P_{\mathrm{e},i}(\theta) - D_i q\,, \qquad i \in \mathcal{V}_I\,, \tag{3.6b}$$

$$k\dot{q} = \frac{\sum_{j\in\mathcal{V}_I} D_j\dot{\theta}_j}{\sum_{j\in\mathcal{V}_I} D_j}\,. \tag{3.6c}$$

Notice that equation (3.6c) in the transformed system can be implemented as a *centralized integrator*. For these reasons, we refer to the controller (2.5b), (3.3) with the choice of gains (3.4) as the centralized-averaging proportional-integral (CAPI) controller. This perspective is not only insightful and shows the communication complexity of the CAPI controller (3.3)-(3.4), but equations (3.6) are also convenient for a stability analysis.

In a first step, we show that the only possible synchronization frequency for any synchronized solutions of the CAPI-controlled system (3.5) is zero. Consequently, synchronized solutions are necessarily obtained by looking for equilibria of (3.5).

Lemma 3.2.1. ***Synchronization Frequency is Zero.***
If the frequencies of the inverters in the CAPI-controlled system (3.5) *are synchronized, then the synchronization frequency is zero.*

Proof. Assume there exists a solution $(\bar{\theta},\bar{p}) \in \Delta_G(\gamma) \times \mathbb{R}^{n_I}$ for the system (3.5) such that the trajectory $\bar{\theta} : \mathbb{R}_{\geq 0} \to \Delta_G(\gamma)$ is synchronized with $\dot{\bar{\theta}} = \bar{\omega}_{\mathrm{sync}}\mathbf{1} \in \mathbb{R}^{n_I}$ and the secondary control input $\bar{p} : \mathbb{R}_{\geq 0} \to \mathbb{R}^{n_I}$ is a time-varying function.

Equation (3.5b) becomes $D_i\overline{\omega}_{\text{sync}} = P_i^* - \overline{p}_i - P_{\text{e},i}(\bar{\theta})$ for all $i \in \mathcal{V}_I$. The terms $D_i\overline{\omega}_{\text{sync}}$ and P_i^* are constant for each $i \in \mathcal{V}_I$. Note that also the power flow $P_{\text{e},i}(\bar{\theta}) = \sum_{j=1}^{n} E_i E_j \left|Y_{ij}\right| \sin(\bar{\theta}_i - \bar{\theta}_j - \phi_{ij})$ is constant for each $i \in \mathcal{V}_I$ for synchronized $\bar{\theta}$ since $\dot{\bar{\theta}}_i - \dot{\bar{\theta}}_j = \overline{\omega}_{\text{sync}} - \overline{\omega}_{\text{sync}} = 0$ for all $i,j \in \mathcal{V}_I$. Therefore, also $\overline{p}_i$ is constant for each $i \in \mathcal{V}_I$ in synchronized state.

In steady state we obtain $0 = k_i \dfrac{\dot{\overline{p}}_i}{D_i} = \dfrac{\sum_{j\in\mathcal{V}_I} D_j}{\sum_{j\in\mathcal{V}_I} D_j}\overline{\omega}_{\text{sync}}$ for $i \in \mathcal{V}_I$. Thus, $\overline{\omega}_{\text{sync}}$ must be zero. □

In a second step, we present a necessary and sufficient parametric condition for the local existence, uniqueness (modulo rotational symmetry) and exponential stability of an equilibrium of the CAPI-controlled system (3.5) for a lossless acyclic network. We also show that the CAPI controller preserves the proportional power sharing.

Theorem 3.2.2. ***Stability of CAPI-Controlled Network.***
Consider a lossless acyclic network of droop-controlled inverters and loads in which all inverters can communicate and average their frequencies, as described by the closed-loop system (3.5) with parameters $k > 0$, $P_i^* \in [0,\overline{P}_i]$, and $D_i > 0$ for $i \in \mathcal{V}_I$. The following two statements are equivalent:

(i) ***Stability of Droop Controller:*** *The droop control stability condition (2.8) holds; and*

(ii) ***Stability of CAPI Controller:*** *There exists an arc length $\gamma \in [0,\pi/2[$ such that the system (3.5) possesses a locally exponentially stable and unique[†] equilibrium $(\dot{\theta}^*, p^*) \in \Delta_G(\gamma) \times \mathbb{R}^{n_I}$.*

If the equivalent statements (i) and (ii) hold true, then θ^* lives on the same synchronization manifold as the solution from Theorem 2.5.1 (ii), and $p_i^* = D_i\omega_{\text{avg}}$ for $i \in \mathcal{V}_I$. Moreover, if the droop coefficients are selected proportionally, then the CAPI controller (3.3)-(3.4) preserves the proportional power sharing property of the primary controller (2.5b).

Proof. We start by writing the closed loop (3.6) in vector form analogous to [30]. Let $D_I = \text{diag}(\{D_i\}_{i\in\mathcal{V}_I})$, and let $D_{\text{tot}} = \sum_{i\in\mathcal{V}_I} D_i = \mathbf{1}^T D_I \mathbf{1}$. Let $\widetilde{P} = (\widetilde{P}_L^T, \widetilde{P}_I^T)^T$, and accordingly let $P_e(\theta) = (P_{e,L}(\theta)^T, P_{e,I}(\theta)^T)^T$, where $P_{e,I}(\theta)$ and $P_{e,L}(\theta)$ are vectors of the lossless power injections (2.4) at the

[†]Modulo the rotational symmetry inherent in the model.

inverters $\mathcal{V}_I$ and the loads $\mathcal{V}_L$. Let the angles be partitioned accordingly as $\theta = (\theta_L, \theta_I)$. With this notation, the closed-loop dynamics (3.6) read in vector form as

$$\underbrace{\begin{bmatrix} I & \mathbf{0} & \mathbf{0} \\ \mathbf{0} & D_I & \mathbf{0} \\ \mathbf{0} & \mathbf{0} & k \cdot D_{\text{tot}} \end{bmatrix}}_{\triangleq Q_1} \begin{bmatrix} \mathbf{0} \\ \dot{\theta}_I \\ \dot{q} \end{bmatrix} = \begin{bmatrix} I & \mathbf{0} & \mathbf{0} \\ \mathbf{0} & I & D_I \mathbf{1} \\ \mathbf{0} & \mathbf{1}^T & D_{\text{tot}} \end{bmatrix} \begin{bmatrix} \widetilde{P}_L - P_{e,L}(\theta) \\ \widetilde{P}_I - P_{e,I}(\theta) \\ -q \end{bmatrix}$$

$$= \underbrace{\begin{bmatrix} I & \mathbf{0} & \mathbf{0} \\ \mathbf{0} & D_I & \mathbf{0} \\ \mathbf{0} & \mathbf{0} & 1 \end{bmatrix}}_{\triangleq Q_2} \underbrace{\begin{bmatrix} I & \mathbf{0} & \mathbf{0} \\ \mathbf{0} & D_I^{-1} & \mathbf{1} \\ \mathbf{0} & \mathbf{1}^T & D_{\text{tot}} \end{bmatrix}}_{\triangleq Q_3} \underbrace{\begin{bmatrix} \widetilde{P}_L - P_{e,L}(\theta) \\ \widetilde{P}_I - P_{e,I}(\theta) \\ -q \end{bmatrix}}_{\triangleq x} . \quad (3.7)$$

The matrices Q_1 and Q_2 are nonsingular. The matrix Q_3 is singular with $\ker(Q_3) = [0 \ (D_I \mathbf{1})^T \ -1]^T$ corresponding to decreasing the secondary variable q and increasing all inverter flows accordingly. On the other hand, we have that $[\mathbf{1}^T \ \mathbf{1}^T \ 0]x = 0$ due to balanced injections $\mathbf{1}^T \widetilde{P} = 0$ and symmetry of the flow $\mathbf{1}^T P_e(\theta) = 0$. We conclude that $x \notin \ker(Q_3)$. Thus, possible equilibria of (3.7) are given by $x = 0$, that is, the set of desired equilibria θ^* from (2.7) and $q^* = 0$. Equivalently, from Theorem 2.5.1, the equation $x = 0$ is solvable for a unique (modulo rotational symmetry) value $\theta^* \in \Delta_G(\gamma)$ if and only if the parametric condition (2.8) holds.

To establish stability of the equilibrium $(\theta^*, 0)$, we follow the proof strategy of [30, Theorem 8]. Recall that the negative load flow Jacobian $-\partial / \partial \theta \, (\widetilde{P} - P_e(\theta))$ is given by

$$L(\theta^*) = B \operatorname{diag}(\{E_i E_j \left| Y_{ij} \right| \cos(\theta_i^* - \theta_j^*)\}_{\{i,j\} \in \mathcal{E}}) B^T .$$

For $\theta^* \in \Delta_G(\gamma)$, $\gamma \in [0, \pi/2[$, we have $\cos(\theta_i^* - \theta_j^*) \geq \cos(\gamma) > 0$. Consequently, $L(\theta^*)$ is a positive semidefinite Laplacian matrix, see [12, Lemma 2]. Thus, the linearization of the DAE (3.7) about the regular fixed point $(\theta^*, 0)$ results in

$$\frac{\mathrm{d}}{\mathrm{d}t} \begin{bmatrix} \mathbf{0}_{|n_L|} \\ \Delta\theta_I \\ k \Delta q \end{bmatrix} = - \begin{bmatrix} I & \mathbf{0} & \mathbf{0} \\ \mathbf{0} & I & \mathbf{0} \\ \mathbf{0} & \mathbf{0} & (k \cdot D_{\text{tot}})^{-1} \end{bmatrix} Q_2 Q_3 \begin{bmatrix} L_{LL} & L_{LI} & \mathbf{0} \\ L_{IL} & L_{II} & \mathbf{0} \\ \mathbf{0} & \mathbf{0} & 1 \end{bmatrix} \begin{bmatrix} \Delta\theta_L \\ \Delta\theta_I \\ \Delta q \end{bmatrix} ,$$

where we have partitioned the matrix $L(\theta^*)$ according to load nodes $\mathcal{V}_L$ and inverter nodes $\mathcal{V}_I$. We solve the set of n_L algebraic equations as

$\Delta\theta_L = -L_{LL}^{-1}L_{LI}\Delta\theta_I$ and substitute into the dynamics to obtain $\mathrm{d}(\Delta\theta_I)/\mathrm{d}t = -D_I^{-1}L_{\mathrm{red}}(\theta^*)\Delta\theta_I - \Delta q$ where $L_{\mathrm{red}}(\theta^*)$ is the Schur complement of $L(\theta^*)$ with respect to the loads $\mathcal{V}_L$, that is $L_{\mathrm{red}}(\theta^*) = L_{II} - L_{IL}L_{LL}^{-1}L_{LI}$. The Jacobian of the system is thus given by

$$J(\theta^*) = \underbrace{\begin{bmatrix} I & \mathbf{0} \\ \mathbf{0} & (k\cdot D_{\mathrm{tot}})^{-1}\end{bmatrix}}_{\triangleq \widetilde{Q}_1}\underbrace{\begin{bmatrix} D_I^{-1} & \mathbf{1} \\ \mathbf{1}^T & D_{\mathrm{tot}}\end{bmatrix}}_{\triangleq \widetilde{Q}_2}\underbrace{\begin{bmatrix} -L_{\mathrm{red}}(\theta^*) & \mathbf{0} \\ \mathbf{0} & -1\end{bmatrix}}_{\triangleq X}.$$

It is known that $L_{\mathrm{red}}(\theta^*)$ is again a positive semidefinite Laplacian matrix [11, Lemma II.1]. The matrix $\widetilde{Q}_1$ is diagonal and positive definite, and $\widetilde{Q}_2$ is positive semidefinite with $\ker(\widetilde{Q}_2) = [(D_I\mathbf{1})^T \ -1]^T$.

We will proceed via a continuity-type argument. Consider momentarily the perturbed Jacobian $J_\epsilon(\theta^*)$, where $\widetilde{Q}_2$ is replaced by the positive definite matrix $\widetilde{Q}_{2,\epsilon} = \begin{bmatrix} D_I^{-1} & \mathbf{1} \\ \mathbf{1}^T & D_{\mathrm{tot}}+\epsilon\end{bmatrix}$, where $\epsilon > 0$. The eigenvalues of $J_\epsilon(\theta^*)$ are obtained from $\widetilde{Q}_1\widetilde{Q}_{2,\epsilon}Xv = \lambda v$ for some $(\lambda, v) \in \mathbb{C}\times\mathbb{C}^{n_I+1}$. Equivalently, let $y = \widetilde{Q}_1^{-1}v$, then we obtain

$$-\widetilde{Q}_{2,\epsilon}\cdot \mathrm{blkdiag}(L_{\mathrm{red}}, 1/(k\cdot D_{\mathrm{tot}}))\, y = \lambda y$$

By applying the Courant-Fischer Theorem [26] to this generalized eigenvalue problem, we conclude, for $\epsilon > 0$ and modulo rotational symmetry, all eigenvalues λ are real and negative.

Now, consider again the unperturbed case $\epsilon = 0$. Recall that $\ker(\widetilde{Q}_2) = [(D_I\mathbf{1})^T \ -1]^T$, and the image of the matrix $\mathrm{blkdiag}(L_{\mathrm{red}}, 1/(k\cdot D_{\mathrm{tot}}))$ excludes $\mathrm{span}([\mathbf{1}^T \ 0]^T)$. It follows that $\widetilde{Q}_{2,\epsilon}\cdot \mathrm{blkdiag}(L_{\mathrm{red}}, 1/(k\cdot D_{\mathrm{tot}}))\, y$ is zero if only if $y \in \mathrm{span}([\mathbf{1}^T 0]^T)$ corresponding to the rotational symmetry. We conclude that the number of negative real eigenvalues of $J_\epsilon(\theta^*)$ does not change as $\epsilon \searrow 0$. Hence, the equilibrium $(\theta^*, 0)$ of the DAE (3.7) is (again, modulo rotational symmetry) locally exponentially stable.

To show that the CAPI controller conserves the proportional power sharing property of primary control, recall that the CAPI controller preserves the synchronization manifold and hence the power flow of the primary-controlled system. Recall also that proportional power sharing is defined by $P_{\mathrm{e},i}/P_i^* = P_{\mathrm{e},j}/P_j^*$ for all $i,j \in \mathcal{V}_I$. Therefore, the CAPI controller preserves it. □

In a simulation with the general parameters from Table 2.1 and the specific parameters given by Table 3.3, we illustrate the properties of the CAPI controller (3.3)-(3.4). The results are shown in Figure 3.4. Observe that, as shown for the DAPI in controller in Figure 3.2, the frequencies of both inverters return to the rated frequency quickly after the change of load and that power sharing is recovered in steady state.

Table 3.3: Specific parameter values for CAPI controller.

Parameter	Symbol	Value
Sec. Droop Coeff.	k	10^{-6} s

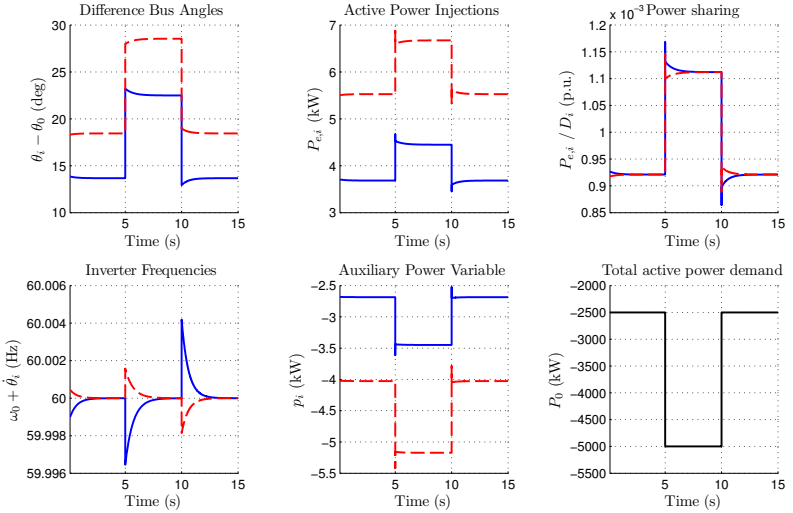

Figure 3.4: CAPI-controlled microgrid consisting of two parallel inverters supplying a load, which changes at $t \in \{5s, 10s\}$.

3.3 Optimal Distributed Averaging PI Control

The selection of the set points and droop coefficients for inverters, following Definition 3, leads to proportional sharing of the load in the primary droop-controlled system (2.5). The DAPI controller (3.2) and the CAPI controller (3.5) are designed in a manner that preserves this proportional sharing. However, a different non-proportional sharing of load between the power generation units might be desired, for example depending on the different generation costs of the different units. In that case a question arises: which control structure and which choice of parameters can lead to some non-proportional desired power injection profile? The work by Andreasson et al. [1] addresses this problem and presents a distributed secondary control algorithm, which aims to regulate the frequency while minimizing a quadratic generation cost in steady state* , that is,

$$\lim_{t\to\infty} u(t) = u^*, \tag{3.8a}$$

$$\{\theta^*, u^*\} = \operatorname*{argmin}_{\theta,u} \sum_{i\in\mathcal{V}} \frac{1}{2} C_i u_i^2 \quad \text{s.t.} \quad u_i = -P_i^* + P_{\mathrm{e},i}(\theta) \quad \forall\, i \in \mathcal{V}\,, \tag{3.8b}$$

where all cost coefficients C_i are strictly positive. Andreasson et al. [1] propose a control algorithm that asymptotically satisfies the optimality conditions (3.8). They also give sufficient parametric conditions for the stability of the linearized power system swing dynamics, based on linear matrix inequalities.

Inspired by [1], we derive *necessary and sufficient* stability and optimality conditions for the nonlinear system dynamics. As in [1], we consider the problem of minimizing the accumulated generation cost:

$$\begin{aligned} \underset{\theta\in\mathbb{T}^n,\, p\in\mathbb{R}^{n_I}}{\text{minimize}} \quad & \sum_{i\in\mathcal{V}_I} \frac{1}{2} C_i p_i^2 \\ \text{subject to} \quad & p_i = -P_i^* + P_{\mathrm{e},i}(\theta) \quad \forall\, i \in \mathcal{V}_I\,, \\ & 0 = -P_i^* + P_{\mathrm{e},i}(\theta) \quad \forall\, i \in \mathcal{V}_L\,, \end{aligned} \tag{3.9}$$

with strictly positive cost coefficients C_i for all $i \in \mathcal{V}_I$.

The optimization problem (3.9) is reminiscent of the optimal generator dispatch problem [19] considered in power transmission networks. Indeed,

*In the problem setup considered in [1], all nodes are adjustable power sources. In (3.8), we omit the distinction of loads $\mathcal{V}_L$ and inverters $\mathcal{V}_I$.

in the absence of a secondary control variable, $p_i = 0$ for all $i \in \mathcal{V}_I$, the optimization problem (3.9), with the set points $P_i^* \in [0, \overline{P}_i]$, $i \in \mathcal{V}_I$, as optimization variables, equals the optimal dispatch problem. If the load demand P_i^* is known exactly for all $i \in \mathcal{V}_L$, then the optimal dispatch problem can be solved a priori and offline to find the optimal inverters set points P_i^*, $i \in \mathcal{V}_I$, see [4], for example. Clearly, this offline solution cannot be adopted if the load is unknown or underlying large time-variations. In the following we show that a careful choice of the droop coefficients in the DAPI controller (3.1) results in a *distributed online optimization procedure* that is adaptive to variable loads.

Notice that, if the droop control stability condition (2.8) holds, then the DAPI controller achieves a stable steady state (θ^*, p^*) of the closed-loop system (3.2) which satisfies the constraints of the optimization problem (3.9), provided that $p_i^* = D_i \omega_{\text{avg}}$, see Theorem 3.1.2. The main result in this chapter shows that this steady state is also a minimizer to the optimization problem (3.9) for the following particular choice of droop coefficients:

$$D_i = \alpha / C_i \quad \forall i \in \mathcal{V}_I \,, \tag{3.10}$$

Here $\alpha \in \mathbb{R}_{>0}$ is the positive and constant *cost-to-droop coefficient*. We arrive at the following result:

Theorem 3.3.1. ***Optimal DAPI control.***
Consider a lossless acyclic network of droop-controlled inverters and loads in which the inverters can communicate through the weighted graph G_c, as described by the closed-loop system (3.2) with parameters $k_i > 0$, $P_i^* \in [0, \overline{P}_i]$, and $D_i > 0$ for $i \in \mathcal{V}_I$, and connected communication Laplacian $L_c \in \mathbb{R}^{n_I \times n_I}$. Consider also the optimization problem (3.9) with coefficients C_i for $i \in \mathcal{V}_I$. Assume that the droop coefficients D_i and optimization coefficients C_i are selected as in (3.10) for some $\alpha \in \mathbb{R}_{>0}$. The following two statements are equivalent:

(i) ***Stability of Droop Controller:*** *The droop control stability condition (2.8) holds; and*

(ii) ***Stability and optimality of DAPI control:*** *There exists an arc length $\gamma \in [0, \pi/2[$ such that the system (3.2) possesses a locally exponentially stable and unique[†] equilibrium $(\theta^*, p^*) \in \Delta_G(\gamma) \times \mathbb{R}^{n_I}$, which minimizes the optimization problem (3.9).*

[†]Modulo the rotational symmetry inherent in the model.

Proof. First notice that the droop coefficients selected as in (3.10) are strictly positive. By Theorem (3.1.2), the closed-loop system (3.2) admits a stable and unique (up to rotational symmetry) solution (θ^*, p^*) if and only if condition (2.8) holds. By Theorem (3.1.2), this solution is (up to rotational symmetry) given by $(\theta^*,p^*) \in \Delta_G(\gamma) \times \mathbb{R}^{n_I}$ for some $\gamma \in [0,\pi/2[$, where the steady state secondary control input is given by

$$p_i^* = D_i \omega_{\text{avg}}\,, \qquad i \in \mathcal{V}_I\,, \tag{3.11}$$

and (θ^*, p^*) satisfy the steady state power flow equation

$$P_i^* - P_{\text{e},i}(\theta^*) - p_i^* = 0\,, \qquad i \in \mathcal{V}_I\,. \tag{3.12}$$

On the other hand, the Lagrangian $\mathcal{L} : \mathbb{T}^n \times \mathbb{R}^{n_I} \times \mathbb{R}^n \to \mathbb{R}$ of the optimization problem (3.9) is given by

$$\mathcal{L}(\theta,p,\lambda) = \sum_{j\in\mathcal{V}_I} \frac{1}{2} C_j p_j^2 + \sum_{j\in\mathcal{V}_I} \lambda_j (p_j - P_j^* + P_{\text{e},j}(\theta)) + \sum_{j\in\mathcal{V}_L} \lambda_j (-P_j^* + P_{\text{e},j}(\theta))\,.$$

Necessary conditions for optimality are given by the KKT conditions [7, 17]:

$$\frac{\partial \mathcal{L}}{\partial \theta_i} = 0 \;:\qquad 0 = \sum_{j\in\mathcal{V}} \left(\lambda_j \cdot \frac{\partial}{\partial \theta_i} \left(P_{\text{e},j}(\theta) \right) \right) \qquad \forall i \in \mathcal{V}\,, \tag{3.13a}$$

$$\frac{\partial \mathcal{L}}{\partial p_i} = 0 \;:\quad C_i p_i = \lambda_i \qquad \forall i \in \mathcal{V}_I\,, \tag{3.13b}$$

$$\frac{\partial \mathcal{L}}{\partial \lambda_i} = 0 \;:\qquad p_i = P_i^* - P_{\text{e},i}(\theta) \qquad \forall i \in \mathcal{V}_I\,. \tag{3.13c}$$

By writing the equations (3.13a) in vector form, we obtain

$$0 = \lambda^{\mathsf{T}} L(\theta)\,, \tag{3.14}$$

where $L(\theta)$ is the load flow Jacobian, that is, the Laplacian matrix with the symmetric weights $-\partial P_{\text{e},i}/\partial\theta_j$. In the lossless case, this matrix is symmetric with $-\partial P_{\text{e},i}/\partial\theta_j = a_{ij}\cos(\theta_i - \theta_j)$, and (3.14) is equivalent to

$$\lambda^{\mathsf{T}} \in \operatorname{span}(\mathbf{1}^{\mathbf{T}})\,.$$

Consequently, we obtain $\lambda_i = \lambda_j = \widetilde{\lambda} \in \mathbb{R}$ for all $i,j \in \mathcal{V}$ and for some $\widetilde{\lambda} \in \mathbb{R}$. Now we can rewrite the KKT conditions from (3.13b)-(3.13c) as

$$p_i = \widetilde{\lambda}/C_i \qquad \forall i \in \mathcal{V}_I\,, \tag{3.15a}$$

$$p_i = P_i^* - P_{\text{e},i}(\theta) \qquad \forall i \in \mathcal{V}_I\,, \tag{3.15b}$$

where $\widetilde{\lambda} \in \mathbb{R}$ is arbitrary. Recall the selection (3.10) of the droop coefficients, and notice that equations (3.15a)-(3.15b) and the steady state equations (3.11)-(3.12) coincide with $\widetilde{\lambda} = \alpha \cdot \omega_{\text{avg}}$, $p = p^*$, and $\theta = \theta^*$ (where the equality holds modulo rotational symmetry).*

Finally, note that the cost function $\sum_{i \in \mathcal{V}_I} \frac{1}{2} C_i p_i^2$ is strictly convex on $\mathbb{R}^{n_I}$, the equality constraint is linear in p, and $\theta = \theta^*$ is one of several solutions to the power flow constraint (3.13c), which are all equivalent in the sense that they do not alter the minimal value of the cost function. Thus, the necessary KKT conditions (3.13a)-(3.13c) are also sufficient for optimality. Accordingly, the steady state (θ^*, p^*) minimizes the optimization problem (3.9). □

Remark 3. ***Optimal CAPI control***
Since the DAPI and the CAPI controller lead to the same unique and stable (up to rotational symmetry) steady state $(\theta^*, p^*) \in \Delta_G(\gamma) \times \mathbb{R}^{n_I}$*, the statement and the proof Theorem 3.3.1 apply analogously to the CAPI controller* (3.3). □

Remark 4. ***Injection Constraints***
The selection of droop coefficients following (3.10) *makes a proportional selection of the inverter parameters as defined in Definition 3 not possible for random cost coefficients. Thus, unless the cost coefficient at each inverter is selected inversely proportional to its rating , that is* $C_i = 1/\overline{P}_i$ *for all* $i \in \mathcal{V}_I$*, we loose the equivalence between the injection constraints and the load constraints as defined in Theorem 2.5.2. Therefore, the feasibility of the power injection in steady state depends on the particular choice of the cost coefficients. A simple calculation leads to the necessary condition*

$$0 \leq P_i^* - \frac{1}{C_i} \frac{\sum_{i \in \mathcal{V}} P_i^*}{\sum_{i \in \mathcal{V}_I} 1/C_i} \leq \overline{P}_i \quad \forall\, i \in \mathcal{V}_I\,.$$

□

The following simulation scenario uses the general parameters listed in Table 2.1 (except of the droop coefficients) and the optimal DAPI parameters listed in Table 3.4. The simulation in Figure 3.5 illustrates the properties of the optimal DAPI controller (3.1),(3.10). Observe that the frequencies of both inverters are brought back to the rated frequency quickly after the change of load. Whereas power sharing is not conserved, $C_1 \cdot p_1$ and $C_2 \cdot p_2$ converge to the same value, which corresponds to the optimality condition (3.15a).

*Notice that $\theta^* \in \Delta_G(\gamma)$ is only one of several choices of $\theta \in \mathbb{T}^n$, which all satisfy the constraint (3.15b) and achieve the same cost. As shown in [3, 30], for the given acyclic network only the choice $\theta = \theta^*$ (modulo rotational symmetry) yields a locally exponentially stable solution.

Table 3.4: Specific parameter values of optimal DAPI controller.

Parameter	Symbol	Value
Sec. Droop Coeff.	k_i	10^{-6} s
Cost Coeff.	$[C_1,C_2]$	[1,2] (p.u)
Cost-to-droop Coeff.	α	4000 s
Comm. Graph	G_{comm}	Two nodes, one edge
Comm. Laplacian	L_c	$(10^4\,\text{Ws}) \cdot \begin{bmatrix} 1 & -1 \\ -1 & 1 \end{bmatrix}$

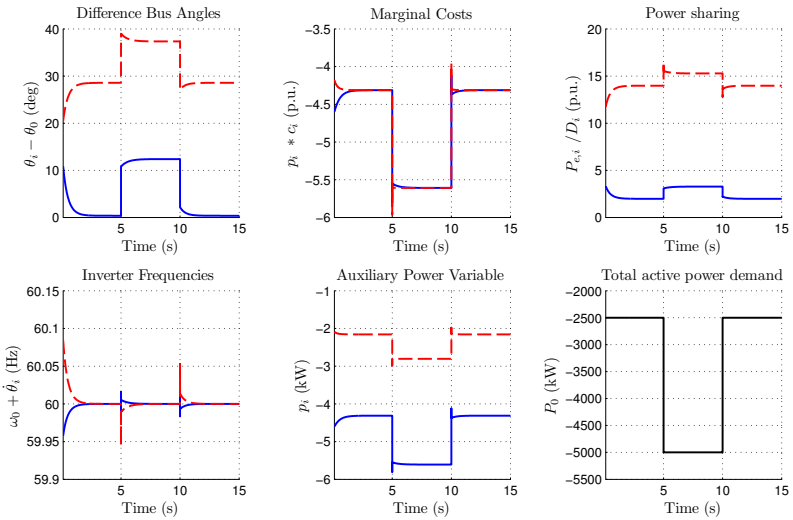

Figure 3.5: Optimal DAPI-controlled microgrid consisting of two parallel inverters supplying a load, which changes at $t \in \{5s,10s\}$.

4 Extensions to Secondary Control

4.1 Extension of DAPI/CAPI Control to Lossy Networks

The assumption of lossless active power transfer simplifies the analysis of power networks, which gives sharp parametric conditions for angle stability (2.8). However, this assumption is not satisfied for low and medium voltage networks, since the subtransmission and the distribution lines are characterized by nonzero R/X ratios (resistance over reactance). On the other hand, our simulations in Section 2.6 and Chapter 3 have shown that the presented primary and secondary controller algorithms succeed in achieving synchronization to the rated frequency in presence of losses in the network. The same simulations with conductances up to three times higher than the conductances from Table 2.1 also demonstrate the successful operation of the primary and secondary controllers.

In this section we remove the assumption of a lossless AC network and analyze the operation of the DAPI controller and the operation of the CAPI controller when the network contains transfer conductances.

Recall that the dynamics of the primary-controlled system are given – here in vector notation – by

$$D\dot{\theta} = P^* - P_e(\theta)\,, \tag{4.1}$$

where $D = \mathrm{diag}(\mathbf{0}_{n_L}, \{D_i\}_{i\in\mathcal{V}_I})$.

4.1.1 Existence and Uniqueness of Synchronized Solutions

The question of existence of a synchronized and stable equilibrium and the uniqueness of the synchronization-manifold for the system (4.1) is considerably more challenging in the lossy case than in the lossless case. Indeed, observe that the power flow from node i to node j, given by $E_i E_j \left|Y_{ij}\right| \sin(\theta_i - \theta_j - \phi_{ij})$, is not the same as the power flow from j to i for non-zero ϕ_{ij}. Thus, the power flow is not symmetric and the power injections do not sum up to zero over all nodes in the network. Therefore,

the techniques used in the proofs of [30, Theorem: 8] and of Theorem 3.2.2 do not generalize.

Due to the lack of simple and sharp parametric conditions for the existence, uniqueness, and stability of synchronized solutions in lossy networks, we *assume* the existence of a unique solution (modulo rotational symmetry) to the primary-controlled system (4.1) and use this assumption to study the secondary-controlled systems (3.2) and (3.5).

Assumption 1. ***Existence and Uniqueness for Primary-Controlled Lossy Network.***
There exists an arc length $\gamma \in [0,\pi/2[$ *such that the closed-loop system* (4.1) *possesses a unique (modulo rotational symmetry) and frequency-synchronized solution* $t \mapsto \theta^*(t) = \left(\theta_o^* + \omega_{\text{sync}}^* t \mathbf{1}_n\right) \pmod{2\pi} \in \Delta_G(\gamma)$, *with* $\omega_{\text{sync}}^* \in \mathbb{R}$ *for all* $t \geq 0$. □

Let Assumption 1 hold. By summing over the equations (4.1) in steady state, we obtain the corresponding unique synchronization frequency

$$\omega_{\text{sync}}^* = \frac{\sum_{i\in\mathcal{V}} P_i^* - \sum_{i\in\mathcal{V}} P_{\text{e},i}(\theta^*)}{\sum_{i\in\mathcal{V}_l} D_i}\,.$$

Therefore, Assumption 1 implies that θ^* is the unique (modulo rotational symmetry) solution in $\Delta_G(\gamma)$ of the algebraic equation

$$P^* - P_e(\theta) - D\,\frac{\sum_{i\in\mathcal{V}} P_i^* - \sum_{i\in\mathcal{V}} P_{\text{e},i}(\theta)}{\sum_{i\in\mathcal{V}_l} D_i}\mathbf{1} = \mathbf{0}\,. \tag{4.2}$$

Before we look for synchronized solutions to the secondary-controlled systems, recall from Lemma 3.1.1 that any synchronized state of the DAPI-controlled system is an equilibrium of (3.2). Analogously, recall from Lemma 3.2.1 that any synchronized state of the CAPI-controlled system is an equilibrium of (3.5)

The following Theorem states the main result of this section; the DAPI and the CAPI controller preserve the unique synchronization-manifold of the primary-controlled system from Assumption 1.

Theorem 4.1.1. ***Existence and Uniqueness of Synchronization Manifolds for DAPI-/CAPI- Controlled systems in Lossy Networks.***
If Assumption 1 holds, then the unique[†] *synchronized solution for the DAPI-controlled system* (3.2) *and the CAPI-controlled system* (3.5) *are given by* $(\theta,p) = (\theta^*, D_I\omega_{\text{sync}}^*\mathbf{1})$.

[†]Modulo the rotational symmetry inherent in the model.

Proof. We have proven in Lemma 3.1.1 and in Lemma 3.2.1 that the only possible synchronization frequency is zero. Therefore, we look only for equilibria of the systems (3.2) and (3.5).

First consider the DAPI-controlled system (3.2); equilibria have to satisfy the equations

$$\mathbf{0} = P^* - P_e(\theta) - \begin{bmatrix} \mathbf{0}_{|\mathcal{V}_L|} \\ p \end{bmatrix}, \tag{4.3a}$$

$$\mathbf{0} = -L_c D_I^{-1} p. \tag{4.3b}$$

In order to satisfy (4.3b), $D_I^{-1}p$ must be in the kernel of the Laplacian L_c and hence must have the form $c\mathbf{1}$ with $c \in \mathbb{R}$. Therefore, every p must have the form $cD_I\mathbf{1}$. Suppose that $(\theta,p) = (\bar{\theta},\bar{\omega}_{\text{sync}} D_I \mathbf{1}) \in \Delta_G(\gamma) \times \mathbb{R}^{n_I}$ satisfies equations (4.3). We have

$$\mathbf{0} = P^* - P_e(\bar{\theta}) - \bar{\omega}_{\text{sync}} D\mathbf{1}. \tag{4.4}$$

By summing over these equations we get

$$\bar{\omega}_{\text{sync}} = \frac{\sum_{i\in\mathcal{V}} P^* - \sum_{i\in\mathcal{V}} P_e(\bar{\theta})}{\sum_{i\in\mathcal{V}} D_i}. \tag{4.5}$$

By inserting (4.5) in equation (4.4), we obtain

$$\mathbf{0} = P^* - P_e(\bar{\theta}) - D\frac{\sum_{i\in\mathcal{V}} P^* - \sum_{i\in\mathcal{V}} P_e(\bar{\theta})}{\sum_{i\in\mathcal{V}} D_i}\mathbf{1},$$

which is identical to (4.2). Assumption 1 implies that θ^* is the unique (modulo rotational symmetry) solution in $\Delta_G(\gamma)$ of (4.2). Therefore, $\bar{\theta}$ lives on $\mathcal{R}_{\theta^*}$, the synchronization manifold of θ^*, $P_e(\bar{\theta}) = P_e(\theta^*)$ and $\bar{\omega}_{\text{sync}} = \omega^*_{\text{sync}}$. It can be verified that $(\theta^*, \omega^*_{\text{sync}} D_I \mathbf{1})$ is an equilibrium of (4.3).

Now, consider the CAPI-controlled system in transformed coordinates (3.6). The equilibria of (3.6) satisfy

$$\mathbf{0} = P^* - D\omega^*_{\text{sync}}\mathbf{1} - P_e(\theta) - Dq\mathbf{1}. \tag{4.6}$$

Suppose that $(\theta,q) = (\widetilde{\theta},\widetilde{\omega}_{\text{sync}}) \in \Delta_G(\gamma) \times \mathbb{R}$ satisfies equations (4.6). Thus, this pair satisfies the equations

$$\mathbf{0} = P^* - P_e(\widetilde{\theta}) - (\widetilde{\omega}_{\text{sync}} + \omega^*_{\text{sync}}) D\mathbf{1}. \tag{4.7}$$

Note that (4.7) is the same as (4.4). By analogous reasoning, we obtain that $\widetilde{\theta} = \theta$ and $\widetilde{\omega}_{\text{sync}} + \omega^*_{\text{sync}} = \omega^*_{\text{sync}}$. A transformation back to the original coordinates leads to the pair $(\theta^*, D_I\omega^*_{\text{sync}}\mathbf{1})$ as the unique (modulo rotational symmetry) equilibrium of (4.6). □

Remark 5. *The results in Theorem 4.1.1 hold without any insight in the closed-form expression of the synchronous solution, knowledge of the synchronization frequency of the primary-controlled system, or knowledge of the magnitudes of the losses. They require only the validity of Assumption 1.* □

4.1.2 Stability of Unique Synchronized Solutions

After we established the existence of unique frequency-synchronization manifolds for the DAPI- and CAPI-controlled systems, we now study the stability properties of solutions on these manifolds. While it is difficult to find a general analytic proof for the stability of synchronized solutions independently of the conductance magnitudes, we can extend the stability from the lossless case using a continuity-type argument for the eigenvalues of the Jacobian.

Theorem 4.1.2. ***Stability of Equilibria for DAPI/CAPI Controllers in Lossy Networks.***
Let Assumption 1 hold and let $(\theta^*, D_I\omega^*_{\text{sync}}\mathbf{1}) \in \overline{\Delta}_G(\gamma) \times \mathbb{R}^{n_I}$ *be the unique synchronized solution of the DAPI-controlled system* (3.2) *and of the CAPI-controlled system* (3.5) *with* $\gamma \in [0, \pi/2[$. *There exists* $\varepsilon > 0$ *such that if* $\|\mathcal{G}\| < \varepsilon$, *the equilibrium given by* $(\theta^*, D_I\omega^*_{\text{sync}}\mathbf{1})$ *is locally exponentially stable for both systems* (3.2) *and* (3.5).

Proof. The lossy DAPI system (3.2) is a smooth perturbation of the nominal lossless DAPI system (3.2). Recall that the eigenvalues of the Jacobian, resulting from the linearization of DAE (3.2) around $(\theta^*, D_I\omega^*_{\text{sync}}\mathbf{1})$ and the elimination of the algebraic equations, are continuous function of the conductances $\mathcal{G}_{ij}$. Notice that conductances do not affect the rotational symmetry, and the Jacobian maintains its zero eigenvalue and associated eigenvector. Since the remaining eigenvalues of the nominal system are in the open left half plane, then – due to continuity and for sufficiently small conductances – the nonzero eigenvalues of the lossy system are also in the open left half plane. The proof goes analogously for the lossy CAPI system (3.5). □

4.1.3 Injection Constraints and Power Sharing in Lossy Networks

Simpson-Porco et al. establish in [30, Theorem 7] an equivalence between the steady-state injection constraints given for all $i \in \mathcal{V}_I$ by

$$0 \leq P_{\mathrm{e},i} \leq \overline{P}_i$$

and the load constraints given by

$$0 \leq -P_L \leq \sum_{j \in \mathcal{V}_l} \overline{P}_j .$$

Since the power injections do not sum up to zero over all nodes – due to the non-symmetric losses in the network – a calculation of an equivalent expression to the injection constraints, similar to the one in [30, Theorem 7], leads to the expression

$$-\sum_{i \in \mathcal{V}} P_{\mathrm{e},i}(\theta^*) \leq -P_L \leq -\sum_{i \in \mathcal{V}} P_{\mathrm{e},i}(\theta^*) + \sum_{j \in \mathcal{V}_l} \overline{P}_j , \tag{4.8}$$

where $\theta^* \in \Delta_G(\gamma)$ with $\gamma \in [0, \pi/2[$ represents the voltage angles in synchronized steady state. Note that this expression depends on the voltage angles in steady state. Thus, it does not represent a general parametric condition for the satisfaction of the injection constraints.

While it is not possible in the lossy case to formulate an equivalence between the injection constraints and load constraints, it turns out that the proportional power sharing properties of the closed loop are maintained in the presence of losses for both the primary- and the secondary-controlled systems.

Theorem 4.1.3. ***Power Sharing in Lossy Networks.***
Let Assumption 1 hold and consider a network of droop-controlled inverters and loads as described by (4.1). The following statements hold:

(i) If the droop coefficients and the set points of the inverters are selected proportionally, that is, the ratios D_i / P_i^* and $P_i^* / \overline{P}_i$ are constant for all $i \in \mathcal{V}$, then the inverters share the load P_L proportionally according to their power ratings, that is, $P_{\mathrm{e},i} / \overline{P}_i = P_{e,j} / \overline{P}_j$, for each $i \in \mathcal{V}$; and

(ii) The secondary controllers DAPI and CAPI, proposed in (3.1) and (3.3)-(3.4), respectively, preserve power sharing.

Proof. The proof of (*i*) is identical to the proof of proportional power sharing in the lossless case, presented in [30, Theorem 7]. To show statement (*ii*), recall that also in the lossy case, both the DAPI and the CAPI controller preserve the synchronization-manifold and hence the power flow of the primary-controlled systems. Therefore, they also preserve the proportional power sharing. □

4.2 Partial DAPI/CAPI Control

The DAPI controller (3.1) requires a connected communication network among the inverters and the CAPI controller (3.1) requires a centralized communication structure among the inverters. Due to physical barriers, to limited or failing communication infrastructure, it may be desirable to have only a subset of inverters within the network assist in regulating the network frequency (see Figure 4.1).

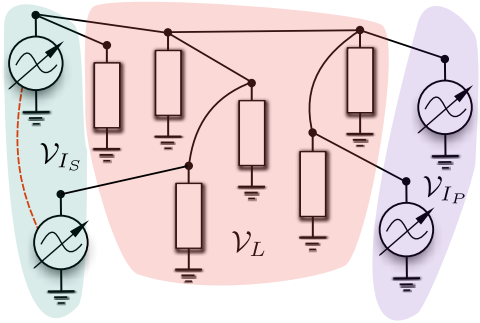

Figure 4.1: Schematic of partial secondary control. The red dotted line represents a communication link.

To investigate this scenario, we partition the set of inverters as $\mathcal{V}_{I_P} \cup \mathcal{V}_{I_S} = \mathcal{V}_I$, where the action of the $\mathcal{V}_{I_P}$ inverters is restricted to primary droop control, and the $\mathcal{V}_{I_S}$ inverters perform the secondary DAPI/CAPI control. Under this partitioning of nodes, the inverter control equations become

$$D_i\dot{\theta}_i = P_i^* - P_{\mathrm{e},i}(\theta)\,, \qquad i \in \mathcal{V}_{I_P}\,, \tag{4.9a}$$

$$D_i\dot{\theta}_i = P_i^* - P_{\mathrm{e},i}(\theta) + u_i(t)\,, \qquad i \in \mathcal{V}_{I_S}\,, \tag{4.9b}$$

The scaled power imbalance is now defined by

$$\omega_{\text{pavg}} \triangleq \sum_{i\in\mathcal{V}} P_i^* \Big/ \left(\sum_{i\in\mathcal{V}_{I_S}} D_i\right) \tag{4.10}$$

4.2.1 Stability of Partial Secondary-Controlled Network

In the following we will show that partial secondary control strategies are able to successfully stabilize the network.

Theorem 4.2.1. ***Stability of Partial Secondary-Controlled Network.*** *Consider an acyclic network of droop-controlled inverters and loads, as described by the closed-loop system (2.5a), (4.9), with parameters $P_i^* \in [0,\overline{P}_i]$ and $D_i > 0$ for $i \in \mathcal{V}_I$. Here, the secondary-control input u_i is defined by either (3.1) (DAPI) or (3.3)-(3.4) (CAPI) for all $i \in \mathcal{V}_{I_S}$ with $k > 0$ and $k_i > 0$. The following two statements are equivalent:*

(i) ***Stability of Droop Controller:*** *The droop control stability condition (2.8) holds; and*

(ii) ***Stability of the Secondary Controllers:*** *There exists an arc length $\gamma \in [0,\pi/2[$ such that the closed-loop system (2.5a), (4.9), (3.1) (respectively, (2.5a), (4.9), (3.3)-(3.4)) possesses the same locally exponentially stable and unique[†] equilibrium $\left(\theta^*, p^*\right) \in \Delta_G(\gamma) \times \mathbb{R}^{|\mathcal{V}_{I_S}|}$.*

If the equivalent statements (i) and (ii) hold true, then θ^* lives on the same synchronization manifold as the solution from Theorem 2.5.1 (ii) and $p_i^* = D_i\omega_{\text{pavg}}$ for $i \in \mathcal{V}_{I_S}$.

Proof. The proof for partial DAPI control (resp. partial CAPI control) is analogous to the proof of [30, Theorem 8] (resp. Theorem 3.2.2), while carefully accounting for the partition $\mathcal{V}_I = \mathcal{V}_{I_P} \cup \mathcal{V}_{I_S}$ in the Jacobian matrices. □

4.2.2 Injection Constraints and Power Sharing

We now investigate the injection constraints and the power sharing properties of the partial DAPI/CAPI control schemes. The steady-state power injection

[†]Modulo the rotational symmetry inherent in the model.

at the equilibrium (θ^*, p^*) is

$$\begin{aligned} P_{\mathrm{e},i}(\theta^*) &= P_i^*, && i \in \mathcal{V}_{I_P} \cup \mathcal{V}_L\,, \\ P_{\mathrm{e},i}(\theta^*) &= P_i^* - D_i\omega_{\mathrm{sync}}, && i \in \mathcal{V}_{I_S}\,. \end{aligned}$$

From the first of these equations, we see that inverters in $\mathcal{V}_{I_P}$ are effectively negative loads. Let $\widetilde{\mathcal{V}}_L = \mathcal{V}_{I_P} \cup \mathcal{V}_L$ be the set of loads in steady state and $\widetilde{\mathcal{V}}_I = \mathcal{V}_{I_S}$ be the set of inverters. By applying [30, Theorem 7] to the modified sets $\widetilde{\mathcal{V}}_I$ and $\widetilde{\mathcal{V}}_L$ gives the following result.

Theorem 4.2.2. ***Injection Constraints and Power Sharing.***
Consider the same setup as in Theorem 4.2.1, and define the total load by $P_L \triangleq \sum_{i\in\mathcal{V}_L} P_i^*$. *If the droop coefficients and the set points of the inverters that perform secondary control are selected proportionally, meaning that the ratios* D_i/P_i^* *and* $P_i^*/\overline{P}_i$ *are constant for all* $i \in \mathcal{V}_{I_S}$, *then the following two statements are equivalent:*

(i) ***Injection Constraints****:* $0 \le P_{e,i}(\theta^*) \le \overline{P}_i \quad \forall i \in \mathcal{V}_I\,.$

(ii) ***Load and Set Point Constraints****:*

$$\begin{aligned} &\sum_{j\in\mathcal{V}_{I_P}} P_j^* \le -P_L \le \sum_{j\in\mathcal{V}_{I_P}} P_j^* + \sum_{j\in\mathcal{V}_{I_S}} \overline{P}_j\,, \\ &0 \le P_i^* \le \overline{P}_i \quad \forall i \in \mathcal{V}_{I_P}\,. \end{aligned}$$

Moreover, the inverters performing secondary control share the load residual $P_L - \sum_{i\in\mathcal{V}_{I_P}} P_i^*$ *proportionally according to their power ratings, i.e.,* $P_{\mathrm{e},i}/\overline{P}_i = P_{e,j}/\overline{P}_j$ *for all* $i \in \mathcal{V}_{I_S}$.

The next simulation, whose results are shown in Figure 4.2, illustrates the existence of a frequency-synchronized steady state for the partial DAPI-controlled system (4.9). Instead of the general setup presented in Section 2.6, we consider a network consisting of four parallel inverters connected to a time-varying load. Two of those inverters are connected via a connected communication graph G_{c} (see Figure 4.1). Table 4.1 contains the simulation parameters. Note that we neglect losses in order to facilitate choosing inverter parameters that would satisfy the injection constraints.

Figure 4.2 shows that the frequencies of the inverters performing secondary control (blue and green) converge rapidly to the synchronization frequency; then follow the frequencies of all other inverters. Figure 4.2 also illustrates the proportional power sharing among the inverters of each

subset. Moreover, observe that the power is shared proportionally among all inverters for the nominal load; this is due to our choice of parameters: we chose proportional droop coefficients for all inverters in both the sets $\mathcal{V}_{I_P}$ and $\mathcal{V}_{I_S}$, following Definition 3, and we chose the set points of the inverters in $\mathcal{V}_{I_P}$, such that they equal the nominal load.

Table 4.1: Parameter values for partial DAPI.

Parameter	Symbol	Value
Nom. Frequency	$\omega^*/2\pi$	60 Hz
Nom. Voltages	E_i^*	$[120, 122, 121, 124]$ V
Output/Line Induc.	L_i	$[0.7, 0.5, 0.6, 0.9]$ mH
Output/Line Resist.	R_i	$[0, 0, 0, 0]\,\Omega$
Inv. Ratings (P)	$P_i^* = \overline{P}_i$	$[2, 3, 1, 1.5]$ kW
Load (P)	$P_0^*(t)$	$P_0^* \in \{-2.5, -5\}$kW
Load (Q)	$Q_0^*(t)$	$Q_0^* \in \{-.5, -1\}$kvar
ω–Droop Coeff.	D_i	$[4, 6, 2, 3] \times 10^3$ W $\cdot$ s
Quadratic E–Droop Coeff.	C_i	$[1, 1, 1, 1]\ 10^3$ s
Quadratic E–Droop Int. Coeff.	τ_i	$[5, 5, 5, 5]$ s
Sec. Droop Coeff.	k_i	$[1,1]10^{-6}$ s
Comm. Graph	G_{comm}	Two nodes, one edge
Comm. Laplacian	L_{c}	$(10^4\,\text{Ws}) \cdot \begin{bmatrix} 1 & -1 \\ -1 & 1 \end{bmatrix}$

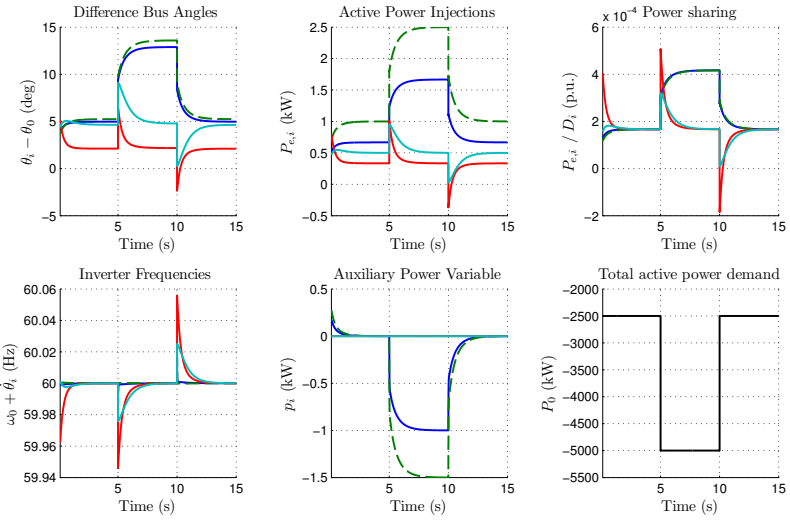

Figure 4.2: Partial DAPI-controlled microgrid consisting of five parallel inverters supplying a load, which changes at $t \in \{5s, 10s\}$.

5 Conclusions

5.1 Summary

The purpose of secondary control in microgrids is to regulate the inverters frequencies to the rated frequency. The main requirements are ensuring the desired power sharing profile (e.g. proportional load sharing or cost minimizing load sharing), satisfactory response to changes in the load, robustness to losses and voltage fluctuations in the network, and a minimal communication complexity.

In this work, we have reviewed the properties of the Distributed Averaging PI (DAPI) controller and presented a nonlinear analysis of the Centralized Averaging PI (CAPI) controller. We have proven that both controllers succeed in regulating the inverters frequencies and ensuring proportional power sharing among the inverters, and illustrated this by the means of simulations. We have also shown that both controllers feature some robustness to losses in the network. Furthermore, our simulations suggested robustness to unmodeled voltage dynamics. Moreover, we could prove that reducing the communication structure to a connected subset of the inverters does not affect the ability of the controllers to achieve synchronization and proportional power sharing among the inverters performing secondary control. Finally, both the DAPI and the CAPI controller minimize a given quadratic cost of secondary-power generation when the droop coefficients of the inverters are selected inverse proportionally to their assigned cost coefficients.

5.2 Possible Future Work

The formulation of sharp parametric conditions for the existence and stability of a synchronized steady state in a lossy primary-controlled microgrid is a challenging and open problem. It can be proven that the secondary controllers DAPI and the CAPI are correctly implemented, that is, they regulate the system frequency of a stable primary-controlled system to its nominal value in the presence of arbitrary losses. However, a stability analysis without any assumptions on the conductances magnitudes is also

a challenging and open problem. Moreover, it remains unclear whether conventional droop control is suitable in general for the stabilization of a dominantly resistive microgrid.

A further interesting task may be to incorporate voltage-droop control and to find parametric condition for the existence and stability of a synchronized steady state of the whole coupled frequency- and voltage-droop-controlled system.

List of Figures

2.1 Primary-controlled microgrid consisting of two parallel inverters supplying a load, which changes at $t \in \{5s, 10s\}$. . . . 14

3.1 Schematic of secondary control. The red dotted line represents a communication link [30]. 16
3.2 DAPI-controlled microgrid consisting of two parallel inverters supplying a load, which changes at $t \in \{5s, 10s\}$. 19
3.3 A microgrid consisting of two parallel inverters supplying a load, which changes at $t \in \{5s, 10s\}$, controlled by the controller (3.5). 20
3.4 CAPI-controlled microgrid consisting of two parallel inverters supplying a load, which changes at $t \in \{5s, 10s\}$. 25
3.5 Optimal DAPI-controlled microgrid consisting of two parallel inverters supplying a load, which changes at $t \in \{5s, 10s\}$. . . 30

4.1 Schematic of partial secondary control. The red dotted line represents a communication link. 36
4.2 Partial DAPI-controlled microgrid consisting of five parallel inverters supplying a load, which changes at $t \in \{5s, 10s\}$. . . 40

List of Tables

2.1 General parameter values. 14

3.1 Specific parameter values for the DAPI controller. 18
3.2 Specific parameter values for controller (3.3)-(3.4). 20
3.3 Specific parameter values for CAPI controller. 25
3.4 Specific parameter values of optimal DAPI controller. 30

4.1 Parameter values for partial DAPI. 39

Bibliography

[1] M. Andreasson, D. V. Dimarogonas, K. H. Johansson, and H. Sandberg. Distributed vs. centralized power systems frequency control under unknown load changes. In *European Control Conference*, Zürich, Switzerland, July 2013. Accepted.

[2] M. Andreasson, H. Sandberg, D. V. Dimarogonas, and K. H. Johansson. Distributed integral action: Stability analysis and frequency control of power systems. In *IEEE Conf. on Decision and Control*, pages 2077–2083, Maui, HI, USA, December 2012.

[3] A. Araposthatis, S. Sastry, and P. Varaiya. Analysis of power-flow equation. *International Journal of Electrical Power & Energy Systems*, 3(3):115–126, 1981.

[4] E Barklund, Nagaraju Pogaku, Milan Prodanovic, C Hernandez-Aramburo, and Tim C Green. Energy management in autonomous microgrid using stability-constrained droop control of inverters. *Power Electronics, IEEE Transactions on*, 23(5):2346–2352, 2008.

[5] S. Barsali, M. Ceraolo, P. Pelacchi, and D. Poli. Control techniques of dispersed generators to improve the continuity of electricity supply. In *IEEE Power Engineering Society Winter Meeting*, pages 789–794, New York, NY, USA, January 2002.

[6] N. Biggs. Algebraic potential theory on graphs. *Bulletin of the London Mathematical Society*, 29(6):641–683, 1997.

[7] S. Boyd and L. Vandenberghe. *Convex Optimization*. Cambridge University Press, 2004.

[8] M. C. Chandorkar, D. M. Divan, and R. Adapa. Control of parallel connected inverters in standalone AC supply systems. *IEEE Transactions on Industry Applications*, 29(1):136–143, 1993.

[9] L. O. Chua, C. A. Desoer, and E. S. Kuh. *Linear and Nonlinear Circuits*. McGraw-Hill, 1987.

[10] F. Dörfler and F. Bullo. On the critical coupling strength for Kuramoto oscillators. In *American Control Conference*, pages 3239–3244, San Francisco, CA, USA, June 2011.

[11] F. Dörfler and F. Bullo. Kron reduction of graphs with applications to electrical networks. *IEEE Transactions on Circuits and Systems I: Regular Papers*, 60(1):150–163, 2013.

[12] F. Dörfler, M. Chertkov, and F. Bullo. Synchronization in complex oscillator networks and smart grids. *Proceedings of the National Academy of Sciences*, 110(6):2005–2010, 2013.

[13] A. Engler and N. Soultanis. Droop control in lv-grids. In *Future Power Systems, 2005 International Conference on*, pages 6 pp.–6, 2005.

[14] E. C. Furtado, L. A. Aguirre, and L. A. B. Tôrres. UPS parallel balanced operation without explicit estimation of reactive power – a simpler scheme. *IEEE Transactions on Circuits and Systems II: Express Briefs*, 55(10):1061–1065, 2008.

[15] J. M. Guerrero, J. C. Vasquez, J. Matas, M. Castilla, and L. G. de Vicuna. Control strategy for flexible microgrid based on parallel line-interactive UPS systems. *IEEE Transactions on Industrial Electronics*, 56(3):726–736, 2009.

[16] J. M. Guerrero, J. C. Vasquez, J. Matas, L. G. de Vicuna, and M. Castilla. Hierarchical control of droop-controlled AC and DC microgrids–a general approach toward standardization. *IEEE Transactions on Industrial Electronics*, 58(1):158–172, 2011.

[17] W Karush. Minima of functions of several variables with inequalities as side conditions. Master's thesis, University of Chicago, Department of Mathematics., 1939.

[18] F. Katiraei, M.R. Iravani, and P.W. Lehn. Micro-grid autonomous operation during and subsequent to islanding process. *Power Delivery, IEEE Transactions on*, 20(1):248–257, 2005.

[19] P. Kundur. *Power System Stability and Control*. McGraw-Hill, 1994.

[20] R. Lasseter and P. Piagi. Providing premium power through distributed resources. In *Annual Hawaii Int. Conference on System Sciences*, pages 4042–4051, Maui, HI, USA, January 2000.

[21] R.H. Lasseter. Microgrids. In *Power Engineering Society Winter Meeting, 2002. IEEE*, volume 1, pages 305–308 vol.1, 2002.

[22] Y. U. Li and C.-N. Kao. An accurate power control strategy for power-electronics-interfaced distributed generation units operating in a low-voltage multibus microgrid. *IEEE Transactions on Power Electronics*, 24(12):2977–2988, 2009.

[23] Hao Liang, Bong Jun Choi, Weihua Zhuang, and Xuemin Shen. Stability enhancement of decentralized inverter control through wireless communications in microgrids. *Smart Grid, IEEE Transactions on*, 4(1):321–331, 2013.

[24] J. A. P. Lopes, C. L. Moreira, and A. G. Madureira. Defining control strategies for microgrids islanded operation. *IEEE Transactions on Power Systems*, 21(2):916–924, 2006.

[25] R. Majumder, A. Ghosh, G. Ledwich, and F. Zare. Power system stability and load sharing in distributed generation. In *Power System Technology and IEEE Power India Conference*, pages 1–6, New Delhi, India, October 2008.

[26] C. D. Meyer. *Matrix Analysis and Applied Linear Algebra*. SIAM, 2001.

[27] J. Schiffer, A. Anta, T. D. Trung, J. Raisch, and T. Sezi. On power sharing and stability in autonomous inverter-based microgrids. In *IEEE Conf. on Decision and Control*, pages 1105–1110, Maui, HI, USA, December 2012.

[28] J. Schiffer, D. Goldin, J. Raisch, and T. Sezi. Synchronization of droop-controlled autonomous microgrids with distributed rotational and electronic generation. In *IEEE Conf. on Decision and Control*, Florence, Italy, December 2013. Submitted.

[29] Q. Shafiee, J. C. Vasquez, and J. M. Guerrero. Distributed secondary control for islanded microgrids - A networked control systems approach. In *Annual Conference on IEEE Industrial Electronics Society*, pages 5637–5642, Montréal, Canada, October 2012.

[30] J. W. Simpson-Porco, F. Dörfler, and F. Bullo. Synchronization and power sharing for droop-controlled inverters in islanded microgrids. *Automatica*, November 2012. to appear.

[31] J. W. Simpson-Porco, F. Dörfler, and F. Bullo. Voltage stabilization in microgrids using quadratic droop control. In *IEEE Conf. on Decision and Control*, Florence, Italy, December 2013. Submitted.

[32] A. Tuladhar, H. Jin, T. Unger, and K. Mauch. Parallel operation of single phase inverter modules with no control interconnections. In *Applied Power Electronics Conference and Exposition*, pages 94–100, Atlanta, GA, USA, February 1997.

[33] Z. Wang, M. Xia, and M. D. Lemmon. Voltage stability of weak power distribution networks with inverter connected sources. In *American Control Conference*, Washington DC, USA, 2013. Submitted.

[34] B. W. Williams. *Power Electronics: Devices, Drivers, Applications and Passive Components*. McGraw-Hill, 1992.

[35] Q.-C. Zhong. Robust droop controller for accurate proportional load sharing among inverters operated in parallel. *IEEE Transactions on Industrial Electronics*, 60(4):1281–1290, 2013.

[36] Q.-C. Zhong and T. Hornik. *Control of Power Inverters in Renewable Energy and Smart Grid Integration*. Wiley-IEEE Press, 2013.